Journal Pre-proof

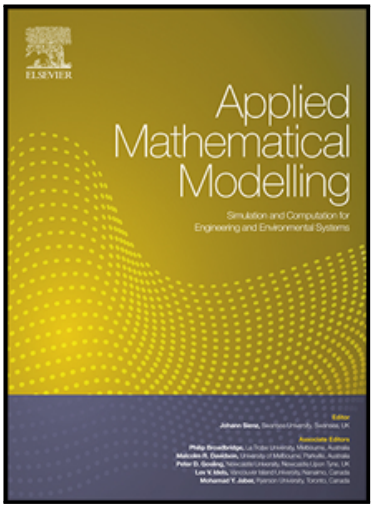

Dynamics of fractional-order multi-beam mass system excited by base motion

Stepa Paunović, Milan Cajić, Danilo Karličić, Marina Mijalković

PII: S0307-904X(19)30740-1
DOI: https://doi.org/10.1016/j.apm.2019.11.055
Reference: APM 13187

To appear in: *Applied Mathematical Modelling*

Received date: 7 June 2019
Revised date: 26 October 2019
Accepted date: 28 November 2019

Please cite this article as: Stepa Paunović, Milan Cajić, Danilo Karličić, Marina Mijalković, Dynamics of fractional-order multi-beam mass system excited by base motion, *Applied Mathematical Modelling* (2019), doi: https://doi.org/10.1016/j.apm.2019.11.055

Highlights

- Transverse vibration of connected beams with attached masses, excited by base motion is investigated
- The beams are connected by fractional viscoelastic layers of Kelvin-Voigt type
- The solution was obtained by the Galerkin approximation, Fourier transform and the impulse system response method
- Frequency response of the system in a steady state vibration regime is analysed
- Several system configurations were considered and the influence of various parameters was investigated

Dynamics of fractional-order multi-beam mass system excited by base motion

Stepa Paunović [a], Milan Cajić [a,], Danilo Karličić [a,b], Marina Mijalković [c]

[a] *Mathematical institute of the Serbian Academy of Sciences and Arts, Kneza Mihaila 36, Belgrade, Serbia*
[b] *College of Engineering, Swansea University, United Kingdom*
[c] *Faculty of Civil Engineering and Architecture, University of Niš, Serbia*

Abstract

Vibration of structures induced by some external sources of excitation is a common phenomenon in many engineering fields such as civil engineering, machinery and aerospace. In most cases, it is desirable to suppress such vibrations but lately there are attempts to exploit this phenomenon for the energy harvesting purposes. Multiple connected structures with attached masses are ideal systems for such applications. In this study, we propose a cantilever multi-beam system excited by base motion, with an arbitrary number of attached masses on beams and fractional-order damping considered. The corresponding governing equations with fractional-order derivatives and non-homogeneous boundary conditions are given. These equations are solved by first homogenizing the boundary conditions and applying the Galerkin discretization, and then using the Fourier transform and impulse response methodology. A steady state response of the system is also analysed. In the numerical study, the influence of various system parameters on the dynamic behaviour of the system is investigated, and different beam-mass configurations are examined. The potential application of this type of systems is also commented.

Keywords: multi-beam system, base excitation, concentrated masses, fractional viscoelasticity, Galerkin method, impulse response

1. Introduction

Systems that can be modelled as multiple connected structural elements such as bars, beams, plates, membranes or wires are very common in engineering practice on micro/nano as well as on macro scale [1, 2]. Application of such systems ranges from civil engineering [3] to mechanical engineering and other applications [4]. It is important to note that multi-beam based systems are commonly employed for energy harvesting purposes based on piezoelectric effect

*Corresponding author
Email address: mcajic@mi.sanu.ac.rs (Milan Cajić)

[5]. Moreover, both the energy harvesting systems with the beams connected in the plane of beams' transverse vibration [6], or in the plane perpendicular to the beam vibration plane [5, 7] are analysed. Also, among others, a very appealing application of energy harvesting devices, based on vibration of beam-like structures, is in civil engineering, particularly on bridges that vibrates due to traffic loads [8–13].

Investigating dynamic properties of a system of multiple connected beams is an important task in the field of structural mechanics and vibration theory. This problem has a long history, where many authors addressed this issue for elastically coupled beams [14–29]. Another interesting problem in vibration of coupled structures is the consideration of system's vibration damping. One among the first papers in this field is a paper by Dublin [30], where two beams were coupled by discrete spring-damper system. In a number of studies, damping is considered in multiple connected structures weather as layer's damping, through continuously distributed spring-damper elements between structures, or by including the internal structural damping through constitutive equations [31–34]. Dynamics of single and multiple connected structures can be significantly affected by the attached concentrated masses or inertia elements [35–38]. A special class of beam-mass problems is the case with the nonhomogeneous boundary conditions, particularly the base excitation problem [39–42]. Attaching concentrated masses to a beam can considerably improve the performance of an energy harvesting system, especially if the piezoelectric effect is used to convert mechanical energy of beam vibrations to electric energy [43].

Damping models of structures based on fractional order derivatives have been extensively used in recent decades. An overview of these works can be seen in a paper by Rossikhin and Shitikova [44], where models of fractional-order viscoelastic coupled beams and plates were also presented. In order to solve linear fractional order differential equations, Kempfle et al. [45] developed the methodology based on functional calculus and Fourier transform. Later, SchÃďfer, and Kempfle [46] suggested the solution for the system of nonhomogeneous fractional order differential equations based on impulse response. In papers by Freundlich [47, 48], previous methodologies served as a tool to solve specific problems of fractional-order base excited viscoelastic beams with and without attached masses. Other authors [49] also observed a similar problem of base excited fractional viscoelastic beams but employed a different methodology to get the responses. In addition, Cajic et al. [50, 51] analysed the beam-mass problem based on nonlocal elasticity and fractional-order damping models using two different approaches. Finally, in a recent study [52], a similar approach was applied to fractional Zener type viscoelastic model.

From everything mentioned previously, it is clear that most of the studies deal separately with multiple coupled structures or single structures with attached masses and base excitation with or without damping considered. The aim of this paper is to present a general model of a fractional-order viscoelastic multi-beam system with attached masses and base excitation as well as a methodology to solve this complex system of nonhomogeneous fractional order differential equations. An impulse response methodology is employed in

conjunction with the Galerkin discretization technique, Fourier transform and residue theory. A general, yet weak damping case is considered in order to decouple the system of equations and solve the corresponding eigenvalue problem. For the purpose of parametric study, different beam-mass configurations are analysed to obtain the responses and show the effects of number of beams, connecting layer properties and mass distribution on vibration amplitudes, and based on these results the potential applications of this type of systems are discussed.

2. Defining the problem

2.1. The problem formulation

In this study, dynamic behaviour of an array of fractional viscoelastic Euler-Bernoulli cantilever beams connected by fractional viscoelastic layers in the plane of beams' transverse vibration is analysed. All the connecting layers in the system have the same material properties. The beams are of constant (but possibly mutually different) geometry and material density. An arbitrary number of concentrated masses can be attached to each of the beams, and each beam is connected to the two neighbouring ones by a lightweight fractional viscoelastic layer. The whole system is subjected to an arbitrary transversal motion of the beams' supports. However, all the supports follow the same motion function. Moreover, all the beams are of the same length L. The described system is schematically presented in Fig. 1. It can be seen that the last and the first beam in the system are connected through fractional viscoelastic layers with fixed bases. Such systems are usually called "Clamped-Chain" systems in the literature. However, the same equations derived in the following text can be applied to a "Free-Chain" system, where the first and the last beam are not connected to a fixed base, which is achieved if the elastic properties of the first and the last fractional viscoelastic layer in the system vanish, that is $\kappa_{(0)} = \kappa_{(N)} = 0$.

Fractional viscoelastic material of the beams is described by the fractional-order Kelvin-Voigt model, which for the (k)-th beam is given as:

$$\sigma_{(k)}(t) = E_k \left(\varepsilon_{(k)}(t) + \tau_1^{\alpha}\, {}_aD_t^{\alpha}\varepsilon_{(k)}(t)\right) \tag{1}$$

where $\sigma_{(k)}(t)$ is the normal stress in the (k)-th beam, $\varepsilon_{(k)}(t)$ is the longitudinal dilatation of the (k)-th beam, and E_k and τ_1^{α} are the relaxed (prolonged, long-time) elasticity modulus and the retardation time of the (k)-th beam material, respectively. Fractional viscoelastic properties of each of the beams are taken to be the same, so consequently, the retardation time τ_1^{α} and the fractional derivative order α are the same for all the beams. In this paper, only the left Riemann-Liouville fractional time derivative of order between the limits of 0 and 1 will be used. This derivative of a function $f(t)$, which is continuous and differentiable on a time interval $[a, b]$, is defined as [53]

$${}_aD_t^{\alpha} f(t) = \frac{1}{\Gamma(n-\alpha)} \frac{d^n}{dt^n} \int_a^t \frac{f(\tau)}{(t-\tau)^{\alpha-n+1}} d\tau, \tag{2}$$

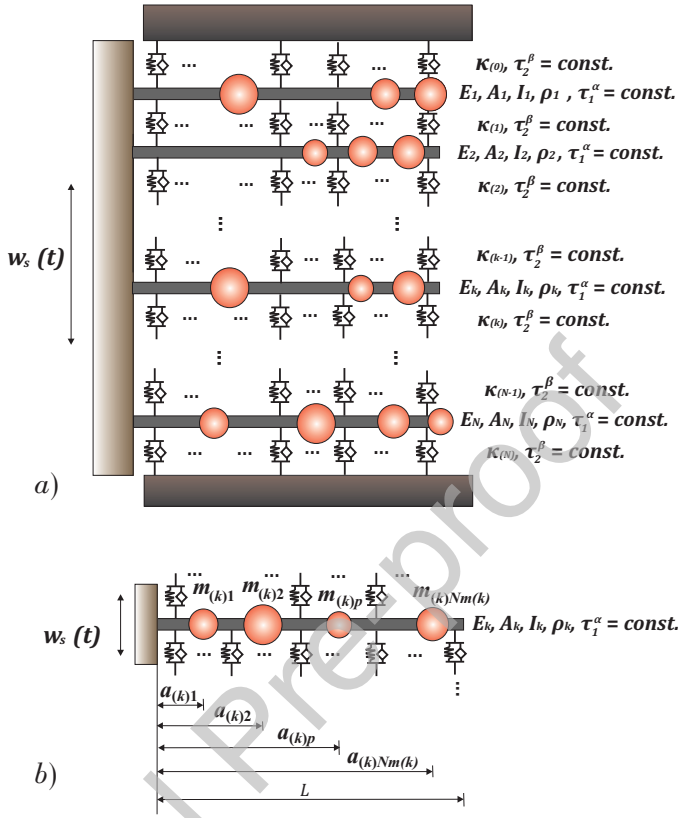

Figure 1: The schematic representation of the considered problem model; a) the whole system of connected beams, b) the (k)-th beam and details of the attached mass positions and notations

where $\alpha \in [0, 1)$ is the derivative order, and $n \in \mathbb{N}$ is a natural number such that $\alpha < n$. In this paper, the notation for the left Riemann-Liouville fractional time derivative will be shortened and it will be denoted by D^α.

In the same manner as the beam material, the material of the interconnecting layers is also modelled by a fractional order Kelvin-Voigt type phenomenological constitutive model, so that the distributed force, representing the influence of the layer between the (k)-th and the $(k+1)$-th beam on the *(k-th)* beam can be expressed as

$$f_{l(k)}(x,t) = \kappa_{(k)}(1 + \tau_2^\beta D^\beta)\left(w_{(k+1)}(x,t) - w_{(k)}(x,t)\right) \tag{3}$$

where $f_{l(k)}(x,t)$ is the distributed force per unit beam length exerted by the (k)-th layer, $\kappa_{(k)}$ and τ_2^β are the relaxed (prolonged, long-time) compliance coefficient and the retardation time of the layer material, respectively, and $w_{(k)}(x,t)$ and $w_{(k-1)}(x,t)$ are the transverse displacements of the (k)-th and the $(k+1)$-th

beam, respectively. As already mentioned, material properties of each interconnecting layer are taken to be the same, so that the compliance coefficient $\kappa_{(1)} = \kappa_{(1)} = \cdots = \kappa_{(N)} = \kappa$ and the retardation time τ_2^β for each layer are the same. However, the indices for the compliance coefficients will be kept in order to emphasize the layer from which the particular influence originates, although the value of this coefficient is the same for each layer.

2.2. The equation of motion

By using the Hamilton's principle [48, 54, 55] the following equation of motion can be formulated for the whole system of N connected beams:

$$\begin{aligned} E_k I_k (1 + \tau_1^\alpha D^\alpha) w_{(k)}'''' + \left(\rho_k A_k + \sum_{p=1}^{N_{m(k)}} m_{(k)p} \delta(x - a_{(k)p}) \right) \ddot{w}_{(k)} - \\ - \kappa_{(k)} (1 + \tau_2^\beta D^\beta)(w_{(k+1)} - w_{(k)}) + \\ + \kappa_{(k-1)} (1 + \tau_2^\beta D^\beta)(w_{(k)} - w_{(k-1)}) = 0 \, ; \quad k = 1, 2, \ldots, N \end{aligned} \tag{4}$$

where $w_{(k)}(x,t)$, I_k, ρ_k and A_k are the transversal displacement, cross-sectional moment of inertia, the material mass density and the cross-sectional area of the k-th beam, respectively, $x \in [0, L]$ is the axial coordinate, $m_{(k)p}$ is the p-th mass attached to the (k)-th beam, and δ is the Dirac function, τ_2^β is the retardation time of the connecting layers, and $\kappa_{(k)}$ is the relaxed compliance coefficient of the layer between the (k)-th and the $(k+1)$-th beam, while $\kappa_{(k-1)}$ is the relaxed compliance coefficient of the layer between the (k)-th and the $(k-1)$-th beam. It should be pointed out that the equations of motion for the first and the last beam of the system should be different from the equations for the rest of the beams. However, the above equation can be used in the presented form for each of the N beams of the system, if it is noted that $w_{(0)} = w_{(N+1)} \equiv 0$. In this paper, $(\bullet)'$ will be used for $\partial(\bullet)/\partial x$, and $(\dot{\bullet})$ will represent $\partial(\bullet)/\partial t$, while $D^\alpha(\bullet)$ will also be denoted by $(\bullet)^{(\alpha)}$.

The corresponding boundary conditions are

$$w_{(k)}(0,t) = w_s(t) \quad \text{and} \quad w'_{(k)}(0,t) = w''_{(k)}(L,t) = w'''_{(k)}(L,t) = 0 \tag{5}$$

where $w_s(t)$ is the motion function of *all* the supports. For each of the beams, zero initial conditions are adopted.

In order to homogenise the boundary conditions in (5), the *absolute* transversal displacements of the (k)-th beam are presented as a superposition of a rigid body motion of the beam, and the relative beam displacements $(v_{(k)}(x,t))$, measured with respect to the clamped end of the beam , that is:

$$w_{(k)}(x,t) = w_s(t) + v_{(k)}(x,t) \tag{6}$$

since in rigid body motion the movement of all the points of all the beams corresponds exactly to the motion of the supports $w_s(t)$. Taking this consideration into account, Eq.(4) becomes

$$E_k I_k(1+\tau_1^\alpha D^\alpha)v''''_{(k)} + \left(\rho_k A_k + \sum_{p=1}^{N_{m(k)}} m_{(k)p}\delta(x-a_{(k)p})\right)\ddot{v}_{(k)} - \\ -\kappa_{(k)}(1+\tau_2^\beta D^\beta)(v_{(k+1)}-v_{(k)}) + \\ +\kappa_{(k-1)}(1+\tau_2^\beta D^\beta)(v_{(k)}-v_{(k-1)}) = F_{(k)}\ ; \quad k=1,2,\ldots,N \tag{7}$$

where $F_{(k)} = F_{(k)}(x,t) \equiv -\left(\rho_k A_k + \sum_{p=1}^{N_{m(k)}} m_{(k)p}\delta(x-a_{(k)p})\right)\ddot{w}_s\ ; \quad k = 1,2,\ldots,N$.

The according boundary conditions are now homogeneous:

$$v_{(k)}(0,t) = v'_{(k)}(0,t) = v''_{(k)}(L,t) = v'''_{(k)}(L,t) = 0 \tag{8}$$

3. Application of the Galerkin method

3.1. The approximate solution for the relative displacements

The exact solution for the relative displacements for each beam of the system can be approximated by a series

$$v_{(k)}(x,t) \approx \sum_{i=1}^{n} \phi_{(k)i}(x) q_{(k)i}(t)\ ; \quad k=1,2,\ldots,N \tag{9}$$

where n is the number of terms in the Galerkin series approximation, $\phi_{(k)i}(x)$ are the trial functions, and $q_{(k)i}(t)$ are some yet undetermined time functions. The trial functions $\phi_{(k)i}(x)$ will be determined later, but for the time being, it will be assumed that they are known.

Introducing the above approximation into Eq.(7) gives:

$$\sum_{i=1}^{n} E_k I_k(1+\tau_1^\alpha D^\alpha)\phi''''_{(k)i} q_{(k)i} + \sum_{i=1}^{n}\left(\rho_k A_k + \sum_{p=1}^{N_{m(k)}} m_{(k)p}\delta(x-a_{(k)p})\right)\phi_{(k)i}\ddot{q}_{(k)i} - \\ -\sum_{i=1}^{n}\kappa_{(k)}(1+\tau_2^\beta D^\beta)(\phi_{(k+1)i}q_{(k+1)i} - \phi_{(k)i}q_{(k)i}) + \\ +\sum_{i=1}^{n}\kappa_{(k-1)}(1+\tau_2^\beta D^\beta)(\phi_{(k)i}q_{(k)i} - \phi_{(k-1)i}q_{(k-1)i}) - F_{(k)} = R^*_{(k)} \neq 0\ ; \quad k=1,2,\ldots,N \tag{10}$$

Here, $R^*_{(k)}$ denotes a nonzero residual, arising as a consequence of the approximation. Successively multiplying the equation (10) by the trial functions $\phi_{(k)j}(x), \quad j=1,2,\ldots,n$ and integrating over the length of the beam, the following system of n equations is obtained for each of the N beams of the system:

$$
\begin{aligned}
&\sum_{i=1}^{n}\left(\int_0^L E_k I_k \phi''''_{(k)i}\phi_{(k)j}dx\right)(1+\tau_1^\alpha D^\alpha)q_{(k)i}+\\
&+\sum_{i=1}^{n}\left(\int_0^L\left(\rho_k A_k+\sum_{p=1}^{N_{m(k)}} m_{(k)p}\delta(x-a_{(k)p})\right)\phi_{(k)i}\phi_{(k)j}dx\right)\ddot{q}_{(k)i}-\\
&-\sum_{i=1}^{n}\frac{\kappa_{(k)}}{\rho_k A_k}\left(\int_0^L \rho_k A_k\phi_{(k+1)i}\phi_{(k)j}dx\right)(1+\tau_2^\beta D^\beta)q_{(k+1)i}+\\
&+\sum_{i=1}^{n}\frac{\kappa_{(k)}+\kappa_{(k-1)}}{\rho_k A_k}\left(\int_0^L \rho_k A_k\phi_{(k)i}\phi_{(k)j}dx\right)(1+\tau_2^\beta D^\beta)q_{(k)i})-\\
&-\sum_{i=1}^{n}\frac{\kappa_{(k-1)}}{\rho_k A_k}\left(\int_0^L \rho_k A_k\phi_{(k-1)i}\phi_{(k)j}dx\right)(1+\tau_2^\beta D^\beta)q_{(k-1)i}=Q_{(k)_j}(t)\\
&j=1,2,\ldots,n\,;\quad k=1,2,\ldots,N
\end{aligned}
\tag{11}
$$

where

$$
Q_{(k)_j}(t)=\int_0^L \phi_{(k)j}F_{(k)}(x,t)dx,\quad j=1,2,\ldots,n \tag{12}
$$

The matrix form of the above system of equations is given by:

$$
\begin{aligned}
&\left[\left[\mathbf{K}_{(k)_{k-1}}\right]\quad\left[\mathbf{K}_{(k)_k}\right]\quad\left[\mathbf{K}_{(k)_{k+1}}\right]\right]\begin{Bmatrix}\mathbf{q}_{k-1}\\ \mathbf{q}_k\\ \mathbf{q}_{k+1}\end{Bmatrix}+\left[[\mathbf{0}]\quad\left[\mathbf{C}_{\alpha(k)_k}\right]\quad[\mathbf{0}]\right]D^\alpha\begin{Bmatrix}\mathbf{q}_{k-1}\\ \mathbf{q}_k\\ \mathbf{q}_{k+1}\end{Bmatrix}+\\
&+\left[\left[\mathbf{C}_{\beta(k)_{k-1}}\right]\quad\left[\mathbf{C}_{\beta(k)_k}\right]\quad\left[\mathbf{C}_{\beta(k)_{k+1}}\right]\right]D^\beta\begin{Bmatrix}\mathbf{q}_{k-1}\\ \mathbf{q}_k\\ \mathbf{q}_{k+1}\end{Bmatrix}+\\
&+\left[[\mathbf{0}]\quad\left[\mathbf{M}_{(k)_k}\right]\quad[\mathbf{0}]\right]\begin{Bmatrix}\ddot{\mathbf{q}}_{k-1}\\ \ddot{\mathbf{q}}_k\\ \ddot{\mathbf{q}}_{k+1}\end{Bmatrix}=\mathbf{Q}_k\,,\quad k=1,2,\ldots,N
\end{aligned}
\tag{13}
$$

where $\mathbf{q}_k$ is the column vector of n time functions for the (k)-th beam, and all the matrices' elements will be defined momentarily. Here it should be pointed out that each of the submatrices in the above equation is of order $n\times n$, and the complete vector of time functions for each beam is of order $3n\times 1$. However, the total accompanying matrices are of order $n\times 3n$, so that the whole system for the (k)-th beam is still of order n. Elements of the introduced matrices and vectors are given in Appendix 1 for the sake of the text clarity. These expressions are determined for the trial functions $\phi_{(k)i}(x)$ defined in the next subsection.

3.2. Choosing the trial functions

For the Galerkin weighted residual method, the trial functions are taken as the weighting functions, and these trial functions should be a part of the set

of comparison functions, that is, they need to satisfy the according boundary conditions *exactly*, as well as satisfy the orthogonality condition [56]. There are several types of functions that meet these requirements, and here the *mode shape functions* of a cantilever beam *with no concentrated masses attached* will be used as the trial functions.

Since in the stated problem all the beams of the system have the same boundary conditions, they will be approximated by the same trial functions. The mode shape functions for a bare cantilever beam (a cantilever with no masses attached) can be expressed as:

$$\phi_{(k)i}(x) = \sqrt{\frac{1}{\rho_k A_k L}} \left(\cos \bar{\beta}_i x - \cosh \bar{\beta}_i x + \frac{\cos \bar{\beta}_i L + \cosh \bar{\beta}_i L}{\sin \bar{\beta}_i L + \sinh \bar{\beta}_i L} \left(\sin \bar{\beta}_i x - \sinh \bar{\beta}_i x \right) \right) \tag{14}$$

where $\bar{\beta}_i^4 = \bar{\omega}_{(k)i}^2 \frac{\rho_k A_k}{E_k I_k}$ is the $i-$th dimensionless frequency parameter of the bare (k)-th beam, and $\bar{\omega}_{(k)i}$ is the $i-$th natural frequency of the bare (k)-th beam. The constant $\sqrt{1/\rho_k A_k L}$ makes the trial functions mutually orthogonal and mass normalised, while the frequency parameters $\bar{\beta}_i$ can be obtained by solving the well-known frequency equation for a cantilever beam [56].

In order to make the trial functions orthonormal with respect to the beam mass, the following orthogonality conditions were used:

$$\begin{aligned} &\int_0^L \rho_k A_k \phi_{(k)i}(x) \phi_{(k)j}(x) dx = \delta_{ij} \\ &\int_0^L E_k I_k \phi''_{(k)i}(x) \phi''_{(k)j}(x) dx = \bar{\omega}_{(k)i}^2 \delta_{ij} \,, \quad i,j = 1,2,...,n \,; \;\; k = 1,2,...,N \end{aligned} \tag{15}$$

where δ_{ij} is the Kronecker delta.

Accordingly, since the trial functions for all the beams are set to be the same and taking into account the above orthogonality conditions, the expressions for the system matrix and vector elements for the (k)-th beam can be calculated, and these expressions are given in Appendix 1.

3.3. The system equations

Using the notation introduced in Eq.(13), N matrix equations of that type, one for each of the N beams, can be combined into the global matrix equation for the whole system of connected beams, which is of the form:

$$\mathbf{K}\mathbf{q} + \mathbf{C}_\alpha \mathbf{q}^\alpha + \mathbf{C}_\beta \mathbf{q}^\beta + \mathbf{M}\ddot{\mathbf{q}} = \mathbf{Q} \tag{16}$$

where $\mathbf{K}$, $\mathbf{C}_\alpha$, $\mathbf{C}_\beta$ and $\mathbf{M}$ are the stiffness matrix, beam material damping matrix, layer damping matrix and mass matrix of the whole system, respectively, and $\mathbf{q}$ and $\mathbf{Q}$ are the vector of the yet undetermined time functions and the vector of the inertial forces in the whole system. For the sake of visual clarity, the explicit forms of each of these system matrices and vectors have been omitted here, but they are provided in Appendix 2.

Equation (16) represents a system of $n \times N$ coupled non-homogeneous differential equations of fractional order, with fractional time derivatives of order

α and β. This system of equations will be solved for the $n \times N$ time functions $\mathbf{q}$ by using the Fourier transform, and determining first the impulse response of the beams, and then taking the convolution of the thus obtained Green functions with the according inertial forces functions, ultimately providing the total system response of the N coupled beams. After the time functions $\mathbf{q}$ are determined, the displacements of each of the beams can be calculated by using Eq.(9) and Eq.(6)

3.4. The impulse response of the system

If instead of the actual inertial forces, the system is subjected to an impulse load, the actual time functions $\mathbf{q}(t)$ will become the impulse response functions or the Green functions, here denoted by $\mathbf{g}(t) = \{G_1(t), G_2(t), \ldots, G_{n \cdot N}(t)\}^T$. Then the system equation (16) will become

$$\mathbf{K}\mathbf{g}(t) + \mathbf{C}_\alpha \mathbf{g}^\alpha(t) + \mathbf{C}_\beta \mathbf{g}^\beta(t) + \mathbf{M}\ddot{\mathbf{g}}(t) = \boldsymbol{\delta}_m(t) \tag{17}$$

where $\boldsymbol{\delta}_m(t)$ is the unit impulse load vector of order $n \cdot N$, which is a vector with the Dirac delta function representing a unit impulse in every m-th coordinate, $m \in \{1, 2, \ldots, n\}$, and all other elements equal to zero. This should reflect the unit impulse load in the m-th coordinate for each of the N beams of the system, since, according to the problem premises, all the beam supports follow the same motion function.

If the Fourier transform $\hat{f}(\omega)$ of a finite function $f(t)$ is defined as

$$\hat{f}(\omega) := \mathcal{F}(f(t)) := \frac{1}{\sqrt{2\pi}} \int_{-\infty}^{\infty} f(t) e^{-\imath\omega t} dt,$$

then, by taking the Fourier transform of the equation (17), the system becomes

$$\mathbf{A}(\omega)\hat{\mathbf{g}}(\omega) = \mathbf{e}_m \tag{18}$$

where $\mathbf{A}(\omega) = \mathbf{K} + (\imath\omega)^\alpha \mathbf{C}_\alpha + (\imath\omega)^\beta \mathbf{C}_\beta + (\imath\omega)^2 \mathbf{M}$, $\imath$ is the imaginary unit, and $\mathbf{e}_m$ is the Fourier transform of the impulse load vector $\boldsymbol{\delta}_m(t)$, that is, it is a vector of order $n \cdot N$ with a unit in every m-th coordinate and all other elements equal to zero.

Now, the equations in the system expressed by Eq.(18) are still coupled. In the case of general damping, these equations cannot be decoupled in general [45, 57]. If the damping matrices were proportional to mass and/or stiffness matrix of the system, i.e. in the proportional damping case, it would be possible to decouple the equations by using the matrix of eigenvectors of the equivalent elastic system to diagonalise the system matrices and move to the system of natural (principal) coordinates [46, 55].

However, here matrices $\mathbf{C}_\alpha$ and $\mathbf{C}_\beta$ are not actually proportional to matrices $\mathbf{K}$ and $\mathbf{M}$, which can be seen by considering the form of these matrices' elements given in Appendix 1. According to [57], there is a special, yet relatively common case when the mentioned decoupling procedure can also be applied to diagonalise these damping matrices, even in the general damping case. Namely,

if the damping in the system is *relatively small*, then the offdiagonal elements in the damping matrices after transformation to the natural coordinates are also relatively small and can be neglected [57]. This procedure effectively decouples the system equations, so it will be used in further analysis in this paper, while noting that all further considerations are limited to the small damping case.

As it has just been described, in the case of small damping, the system of coupled equations in Eq.(18) can be decoupled by considering the eigenproblem of the corresponding *elastic* system, given by

$$\left(\mathbf{K} - {\omega_r}^2\mathbf{M}\right)\mathbf{u}_r = \mathbf{0}, \qquad r = 1, 2, \ldots . n \cdot N \tag{19}$$

where ω_r is the $r-$th undamped natural frequency of the whole system with N beams (each having n terms in the Galerkin approximation), and $\mathbf{u}_r$ is the $r-$th eigenvector of this elastic system. It should be pointed out that these vectors are mass-normalized and that they satisfy the *generalized* orthogonality conditions.

Now, if the damping was proportional, the matrix of the elastic system eigenvectors $\mathbf{\Phi}$ given by $\mathbf{\Phi} = [\mathbf{u}_1\, \mathbf{u}_2\, \ldots\, \mathbf{u}_{n\cdot N}]$ could be used to directly decouple the system, since it would diagonalise all the system matrices [46]. However, since in the case considered here the damping is not proportional, the matrix of eigenvectors $\mathbf{\Phi}$ diagonalises the system stiffness matrix $\mathbf{K}$ and mass matrix $\mathbf{M}$, but *not* the damping matrices $\mathbf{C}_\alpha$ and $\mathbf{C}_\beta$, that is:

$$\begin{aligned}
\mathbf{M}^{\mathrm{d}} &= \mathbf{\Phi}^{\mathrm{T}}\mathbf{M}\mathbf{\Phi} = \mathbf{I} \\
\mathbf{K}^{\mathrm{d}} &= \mathbf{\Phi}^{\mathrm{T}}\mathbf{K}\mathbf{\Phi} = diag[K^d_{rr}] \\
\mathbf{C}^{\mathrm{d}}_{\alpha} &= \mathbf{\Phi}^{\mathrm{T}}\mathbf{C}_{\alpha}\mathbf{\Phi} \neq diag[C^d_{\alpha rr}] \\
\mathbf{C}^{\mathrm{d}}_{beta} &= \mathbf{\Phi}^{\mathrm{T}}\mathbf{C}_{\beta}\mathbf{\Phi} \neq diag[C^d_{\beta rr}]
\end{aligned} \tag{20}$$

where $\mathbf{I}$ is the identity matrix.

Having this in mind, and if a vector of Fourier transformed decoupled impulse response functions $\hat{\boldsymbol{\eta}}^T(\omega) = [\hat{\eta}_1(\omega), \hat{\eta}_2(\omega), \ldots, \hat{\eta}_n(\omega)]$ is introduced, such that it holds:

$$\hat{\boldsymbol{\eta}}(\omega) = \mathbf{\Phi}^{\mathrm{T}}\hat{\mathbf{g}}(\omega) \qquad \Leftrightarrow \qquad \hat{\mathbf{g}}(\omega) = \mathbf{\Phi}\hat{\boldsymbol{\eta}}(\omega) \tag{21}$$

it can be seen that by multiplying the equation Eq.(18) by $\mathbf{\Phi}^{\mathrm{T}}$ from the left, the following (almost) decoupled system of equations is obtained:

$$\mathbf{A}^{\mathrm{d}}(\omega)\hat{\boldsymbol{\eta}}(\omega) = \mathbf{\Phi}^{\mathrm{T}}\mathbf{e}_m \tag{22}$$

where $\mathbf{A}^{\mathrm{d}}(\omega) = \mathbf{K}^{\mathrm{d}} + (\imath\omega)^{\alpha}\mathbf{C}^{\mathrm{d}}_{\alpha} + (\imath\omega)^{\beta}\mathbf{C}^{\mathrm{d}}_{\beta} + (\imath\omega)^2\mathbf{M}^{\mathrm{d}}$. After neglecting the off-diagonal elements of the transformed damping matrices, each equation of the system (22) can be solved independently, giving the following expression for the r-th decoupled impulse response function:

$$\hat{\eta}_r(\omega) \approx \frac{1}{A^d_{rr}}\sum_{\theta=1}^{n\cdot N}\Phi_{\theta r}e_{\theta} = \frac{\mathbf{u}_r\cdot\mathbf{e}_m}{A^d_{rr}} = \frac{\sum_{b=1}^{N}\Phi_{(b-1)n+m,\,r}}{K^d_{rr} + (\imath\omega)^{\alpha}C^d_{\alpha rr} + (\imath\omega)^{\beta}C^d_{\beta rr} + (\imath\omega)^2M^d_{rr}}, \qquad r = 1, 2, \ldots, n\cdot N \tag{23}$$

To convert the above decoupled Green functions from the frequency-domain to the time-domain, the inverse Fourier transform of the above equation needs to be performed. In order to achieve this, one needs to perform the contour integration and find the singular points (poles) of the above function [45]. This function has two branch points at $s = 0$ and $s = \infty$, and simple poles at the same magnitudes of s for which the denominator of the last term in the above equation vanishes, i.e. for the roots of the corresponding characteristic equation. The characteristic equation for the system considered in this paper can be formulated as

$$s_r^2 + C^d_{\alpha rr} s_r^\alpha + C^d_{\beta rr} s_r^\beta + \omega_r^2 = 0 \,, \qquad r = 1, 2, \ldots, n \cdot N \tag{24}$$

where the change of variables $\imath\omega = s$ and the substitution $\omega_r^2 = K^d_{rr}/M^d_{rr}$ have been introduced.

It can be shown [44] that each of the characteristic equations (24) has two complex conjugate roots $s_{r1,2} = -\varsigma_r \pm i\Omega_r$, with real part of the roots (ς_r) representing the damping ratio, and the imaginary part (Ω_r) representing the damped system frequency. However, due to the presence of fractional exponents, this fractional polynomial equation with arbitrary fractional parameters can be very difficult or even impossible to solve directly by standard numerical methods and available commercial software (such as Wolfram Mathematica for example). Therefore, instead, the following procedure for solving fractional equations with two fractional orders, similar to the one found in [58], is applied.

By introducing the substitution $s = \xi e^{\imath\psi}$, the expression (24) can be separated into real and imaginary parts as:

$$\begin{aligned} \xi_r^2 \cos 2\psi_r + C^d_{\alpha rr} \xi_r^\alpha \cos \alpha\psi_r + C^d_{\beta rr} \xi_r^\beta \cos \beta\psi_r + \omega_r^2 = 0 \\ \xi_r^2 \sin 2\psi_r + C^d_{\alpha rr} \xi_r^\alpha \sin \alpha\psi_r + C^d_{\beta rr} \xi_r^\beta \sin \beta\psi_r = 0 \end{aligned} \tag{25}$$

Now, by introducing the following parameters

$$C^d_{\alpha rr} \xi_r^\alpha = \mathrm{x}_{1r} \quad , \qquad C^d_{\beta rr} \xi_r^\beta = \mathrm{x}_{2r} \tag{26}$$

the previous equation is transformed into

$$\begin{aligned} \xi_r^2 \cos 2\psi_r + \mathrm{x}_{1r} \cos \alpha\psi_r + \mathrm{x}_{2r} \cos \beta\psi_r + \omega_r^2 = 0 \\ \xi_r^2 \sin 2\psi_r + \mathrm{x}_{1r} \sin \alpha\psi_r + \mathrm{x}_{2r} \sin \beta\psi_r = 0 \end{aligned} \tag{27}$$

The two introduced parameters x_{1r} and x_{2r} can take non-negative real values, that is $(\mathrm{x}_{1r}, \mathrm{x}_{2r}) \in \mathbb{R}_0^+$ [58]. These parameters are not independent, which can be seen from Eq.(26):

$$\mathrm{x}_{2r} = C^d_{\beta rr} \left(\frac{\mathrm{x}_{1r}}{C^d_{\alpha rr}} \right)^{\beta/\alpha} \tag{28}$$

Now, for any assumed value of the parameter x_{1r}, and correspondingly x_{2r}, the angle ψ_r can be determined from the transcedental equation obtained by

dividing the second equation of Eq.(25) by the first one, thus eliminating the ξ_r^2, i.e.

$$\tan 2\psi_r = \frac{\sin 2\psi_r + \mathrm{x}_{1r}\sin\alpha\psi_r + \mathrm{x}_{2r}\sin\beta\psi_r}{\cos 2\psi_r + \mathrm{x}_{1r}\cos\alpha\psi_r + \mathrm{x}_{2r}\cos\beta\psi_r + \omega_r^2} \tag{29}$$

The value of ξ_r can now be determined from the second equation in Eq.(27) as

$$\xi_r = \sqrt{-\frac{\mathrm{x}_{1r}\sin\alpha\psi_r + \mathrm{x}_{2r}\sin\beta\psi_r}{\sin 2\psi_r}} \tag{30}$$

However, for arbitrarily chosen values of parameters x_{1r} and x_{2r}, the obtained values of ψ_r and ξ_r do not correspond to the initially introduced values of parameters $C^d_{\alpha rr}$ and $C^d_{\beta rr}$ (that contain fixed retardation times τ_1^α and τ_2^β). Therefore, in order to find the corresponding root of the characteristic equation (Eq.(24)) for the fixed values of $C^d_{\alpha rr}$ and $C^d_{\beta rr}$, the following iterative procedure is performed.

First, assume an initial value for the auxiliary variable x_{1r}. Then, calculate x_{2r} by equation (28), calculate ψ_r by equation (29), and ξ_r by equation (30). After that, calculate the trial value for the damping matrix element corresponding to the considered equation, by equation (26), that is: $C^{d\,trial}_{\alpha rr} = \mathrm{x}_{1r}/\xi_r^\alpha$. Finally, determine the difference between the calculated trial value and the actual value of the corresponding damping matrix element: $\Delta = C^d_{\alpha rr} - C^{d\,trial}_{\alpha rr}$, and compare the calculated difference Δ to a pre-set accuracy limit ϵ. If $|\Delta| > \epsilon$, calculate the new value for x_{1r} as: $\mathrm{x}_{1r}^{next} = (1 + \Delta/C^d_{\alpha rr})\ \mathrm{x}_{1r}^{previous}$ and repeat the iteration from the second step.

The iteration proceeds until the value for the variable x_{1r} corresponding to the given damping matrix element $C^d_{\alpha rr}$ is determined with the desired accuracy. When x_{1r} for the considered $r-$th vibration mode is determined, the corresponding parameters ψ_r and ξ_r can be calculated by equations (29) and (30), after which the r-th root of the characteristic equation is defined by $s_r = \xi_r e^{i\psi_r}$.

Once all the roots of the characteristic equations (24) are known, the decoupled impulse responses $\eta_r(t)$ can be determined. However, as already mentioned, direct inverse Fourier transform of $\hat{\eta}_r(\omega)$ is not so straightforward. Instead, the residuum theory is used, so that the real decoupled impulse responses in time domain can be calculated as [45, 46, 59]

$$\eta_r(t) = K_{1r}(t) + K_{2r}(t) \tag{31}$$

where

$$\begin{aligned} K_{1r}(t) &= \sum_{\mathrm{Re}[s_r]<0} \mathrm{Res}\left[\hat{\eta}_r(s)\, e^{s_r t}\right] = a_{1r} e^{(-\sigma_r t)}\sin(\Omega_r t + a_{2r}) \\ K_{2r}(t) &= \frac{1}{\pi}\int_0^\infty \frac{\Upsilon_r(z) e^{-zt}}{\Psi_r^2(z) + \Upsilon_r^2(z)} dz \end{aligned} \tag{32}$$

Here, the following notations have been used

$$
\begin{aligned}
&a_{1r} = \frac{2}{\sqrt{\varrho_r^2 + \vartheta_r^2}} \sum_{b=1}^{N} \Phi_{(b-1)n+m,r} \quad , \qquad a_{2r} = \arctan\left(\frac{\varrho_r}{\vartheta_r}\right) \\
&\varrho_r = \mathrm{Re}[P'(s)] \\
&\vartheta_r = \mathrm{Im}[P'(s)] \\
&\Psi_r = \mathrm{Re}[P(s)] = \left[z^2 + C^d_{\alpha rr} z^\alpha \cos(\alpha\pi) + C^d_{\beta rr} z^\beta \cos(\beta\pi) + \omega_r^2\right] \\
&\Upsilon_r = \mathrm{Im}[P(s)] = \left[C^d_{\alpha rr} z^\alpha \sin(\alpha\pi) + C^d_{\beta rr} z^\beta \sin(\beta\pi)\right] \\
&P(s) = s^2 + C^d_{\alpha rr} s^\alpha + C^d_{\beta rr} s^\beta + \omega_r^2 \\
&P'(s) \equiv dP(s)/ds = 2s + \alpha C^d_{\alpha rr} s^{\alpha-1} + \beta C^d_{\beta rr} s^{\beta-1}
\end{aligned}
\tag{33}
$$

where the expressions for Ψ_r and Υ_r have been determined from the expression for $P(s)$, by taking the change of variables $s = ze^{\imath\pi}$.

The part $K_{1r}(t)$ of the solution is the residuum, oscillatory part, while $K_{2r}(t)$ is the drift part, which is much smaller than the $K_{1r}(t)$ and diminishes over time [45]. Therefore, $K_{2r}(t)$ will be neglected in numerical analyses conducted in this paper.

After all the decoupled impulse responses $\eta_r(t), \quad r = 1, 2, \ldots, n \cdot N$ are determined, the coupled impulse responses that are being sought $G_i(t), \quad i = 1, 2, \ldots, n \cdot N$ can be calculated as

$$
\mathbf{g}(t) = \mathbf{\Phi}\boldsymbol{\eta}(t) \quad \Leftrightarrow \quad G_i(t) = \sum_{r=1}^{n \cdot N} \Phi_{ir} \eta_r(t) \tag{34}
$$

3.5. The total response of the system

As already mentioned, the total system response is obtained by taking the convolution of the unit impulse system response G_i, and the actual inertial forces load Q_i defined in Eq.(16), which can be stated as

$$
q_i(t) = \int_0^t G_i(t-\tau) Q_i(\tau) d\tau \tag{35}
$$

Now that the time functions $q_i(t)$ are known, the relative transversal displacements of each of the beams can be calculated through Eq.(9), by using the time functions corresponding to that beam. And when relative displacements are known, the absolute displacements of the (k)-th beam can be obtained through Eq.(6), thus providing the solution to the stated problem of transversal vibrations of a system of coupled beams. In addition to this solution, a steady state response of the considered system will also be analysed, so in the next section, the frequency response function for such system will be determined.

4. Frequency response function

Analysis of the steady state response of the system due to a harmonic excitation can be very useful in practical applications of the presented model. In this

section, the frequency response function will be derived by using the methodology similar to the one found in [60], for a system of N connected beams exposed to harmonic movement of supports:

$$w_s(t) = w_0 e^{\imath\,\Omega_F t} \tag{36}$$

where w_0 and Ω_F are the amplitude and the frequency of the support motion function, respectively, and $\imath$ is the imaginary unit.

Having this in mind, and starting at the equation of motion of the system of beams and applying the Galerkin method as described in Section 3, Eq.(12) becomes

$$Q_{(k)i} = \Omega_F^2 w_0\, y_{(k)i}\, e^{\imath\,\Omega_F t}\,, \quad i = 1, 2, \ldots, n\,, \quad k = 1, 2, \ldots N \tag{37}$$

where

$$y_{(k)i} = \left(\int_0^L \rho_k A_k \phi_{(k)i}(x) dx + \sum_{p=1}^{N_{m(k)}} m_{(k)p} \phi_{(k)i}(a_{(k)p}) \right) \tag{38}$$

while for a system in a steady state, the Galerkin approximation of the relative displacements of the beams becomes:

$$v^{ss}_{(k)}(x,t) \approx \sum_{i=1}^{n} \phi_{(k)i}(x) q^{ss}_{(k)i}(t)\,, \quad k = 1, 2, \ldots N \tag{39}$$

where

$$q^{ss}_{(k)i}(t) = u_{(k)i} e^{\imath\,\Omega_F t}\,, \quad i = 1, 2, \ldots n, \quad k = 1, 2, \ldots N \tag{40}$$

are the steady state time functions, with $u_{(k)i}$ being the amplitude of the corresponding time function.

Noting that the fractional derivative of an exponential function can be evaluated as in [59]:

$$D^\gamma q^{ss}_{(k)i}(t) = (\imath\,\Omega_F)^\gamma u_{(k)i} e^{\imath\,\Omega_F t}\,, \qquad \gamma \in \Re \tag{41}$$

for a system in steady state regime Eq.(16) becomes:

$$\mathbf{A}(\Omega_F)\mathbf{u} = \Omega_F^2 w_0 \mathbf{y} \tag{42}$$

where

$$\begin{aligned} \mathbf{A}(\Omega_F) &= \mathbf{K} + (\imath\,\Omega_F)^\alpha \mathbf{C}_\alpha + (\imath\,\Omega_F)^\beta \mathbf{C}_\beta + (\imath\,\Omega_F)^2 \mathbf{M} \\ \mathbf{u}^T &= [\mathbf{u}_1\ \mathbf{u}_2\ \ldots\ \mathbf{u}_N] = \left[u_{(1)1}\ u_{(1)2}\ \ldots\ u_{(1)n}\ u_{(2)1}\ \ldots\ u_{(N)n}\right] \\ \mathbf{y}^T &= [\mathbf{y}_1\ \mathbf{y}_2\ \ldots\ \mathbf{y}_N] = \left[y_{(1)1}\ y_{(1)2}\ \ldots\ y_{(1)n}\ y_{(2)1}\ \ldots\ y_{(N)n}\right] \end{aligned} \tag{43}$$

Now the complex amplitudes of the steady state time functions can be easily determined from the Eq.(42) as:

$$\mathbf{u}(\omega) = \Omega_F^2\, w_0\, \mathbf{A}^{-1}(\Omega_F)\mathbf{y} \tag{44}$$

Introducing this solution into Eq.(40) and then into Eq.(39), the amplitudes of the relative beam displacements can be expressed as:

$$v^{ss}_{(k)_{max}}(x, \Omega_F) \approx \sum_{i=1}^{n} \phi_{(k)i}(x) u_{(k)i}(\Omega_F)\,, \quad k = 1, 2, \ldots N \tag{45}$$

5. Model validation

The exact analytical solution to the problem of transverse vibrations of fractional-order viscoelastic beams carrying attached masses, connected by fractional-order viscoelastic layers and subjected to the support motion has not yet been reported in literature. For this reason, the results of the analytical approximate solution presented in this paper will be validated against the results obtained by the Finite Element Method (FEM), being one of the most thoroughly developed numerical methods. However, the FEM solution was obtained only for a special case with an arbitrary number of *elastic* beams carrying an arbitrary number of attached masses and connected by viscoelastic layers, but *with an integer order damping*, that is, only for $\beta = 1.0$. Nevertheless, the results show that the presented solution adequately describes the influence of the connecting layers and the dynamic behaviour of a single (separated) beam, as well as multiple connected beams. Moreover, the proposed solution will also be validated against the frequency response function derived in the previous section for a steady state vibration regime.

5.1. Validation with the Finite Element Method

For this validation, a case with the following numerical values of the considered parameters was analysed: number of beams: $N = 5$, the cross-sectional area A_k and second moment of inertia I_k for all the beams were taken to be the same and equal to: $A_k = 5 \cdot 10^{-4} m^2$ and $I_k = 1.667 \cdot 10^{-8} m^4$. Length of all the beams: $L = 0.8m$, mass density for all the beams: $\rho_k = 1190.0 kg/m^3$, relaxed elastic modulus $E_k = 3.2 \cdot 10^9 Pa$, number of attached masses per beam: $N_{m(k)} = 3$, each weighting one third of the of a single beam weight. Relaxed compliance coefficient of each interconnecting layer: $\kappa = 200 N/m^2$, retardation time and derivative order for each interconnecting layer: $\tau_2^{\beta} = 0.002\ s^{\beta}$ and $\beta = 1.00$. Moreover, in this validation study, a free chain of beams is considered, which is achieved by setting that $\kappa_0 = \kappa_N = 0\ N/m^2$.

All the supports follow the motion function $w_s(t) = w_0 \sin(\Omega_F t^2/2)$, with: $w_0 = 0.001m$ and $\Omega_F = 20 s^{-2}$. The Galerkin approximation is applied with $n = 3$ terms considered.

For the described case, the damped frequencies of the system are presented in Table 1. Since there are 5 connected beams and 3 considered Galerkin terms, there are 15 system frequencies obtained in total - 3 intermodal groups of 5 intramodal vibration modes (if the terminology found in [27] is adopted). As it can be seen from the table, results obtained by the two methods are in excellent agreement.

In Fig. 2 the relative displacements of the free end of the beams in the first 10 seconds of the motion are presented. Since the geometrical and material properties are set to be the same for each beam, and all the connected beams carry the same number of attached masses of equal weight, the responses of all the beams are identical, so that the presented diagram shows only two curves - the blue continuous line represents the displacements calculated by FEM, while the orange dashed line represents the Galerkin solution.

Table 1: Damped frequencies of a system with 5 connected beams and 3 considered terms in the Galerkin approximation

Intermodal mode	Intramodal mode	Galerkin solution [1/s]	FEM solution [1/s]	Absolute difference [1/s]	Relative difference [%]
1	1	31.212	31.218	-0.00576095	-0.02
	2	31.942	31.947	-0.00563794	-0.02
	3	33.776	33.781	-0.00518899	-0.02
	4	35.913	35.917	-0.00456778	-0.01
	5	37.551	37.555	-0.00402581	-0.01
2	1	195.802	195.000	0.802372658	0.41
	2	195.933	195.129	0.803868333	0.41
	3	196.274	195.468	0.806079751	0.41
	4	196.696	195.886	0.809828038	0.41
	5	197.037	196.224	0.812868898	0.41
3	1	532.953	528.840	4.112818306	0.78
	2	533.000	528.888	4.112338624	0.78
	3	533.126	529.012	4.114048817	0.78
	4	533.280	529.166	4.114445331	0.78
	5	533.405	529.290	4.115199473	0.78

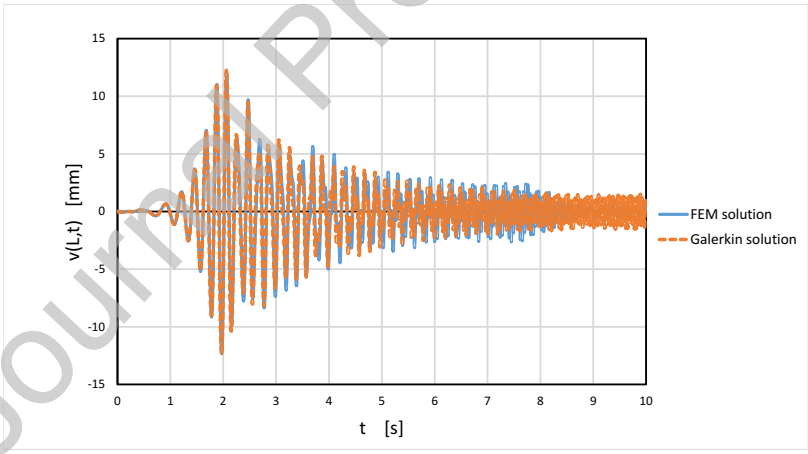

Figure 2: The relative displacements of the free end of a cantilever in the system of $N = 5$ connected beams with $N_{m(k)} = 3$ attached masses and $\beta = 1.0$; blue continuous line - the FEM solution, orange dashed line - the Galerkin solution

As it can be seen from the figure, the results obtained by these two methods are again in very good agreement for a certain initial period of time. However, after some time a slight difference in displacements appears between the FEM solution, obtained via the Newmark method, and the Galerkin solution, obtained via convolution.

5.2. Validation with the frequency response function

In the previous subsection the presented model was validated against the FEM solution, both analysing the system natural frequencies, and its relative displacements as functions of time. Now another approach will be applied. Namely, for the same geometrical and material properties of the beams as in the previous validation analysis, the frequency response function (FRF) will be determined as described in Section 4. After that, the solution derived in Section 3 will be used to determine system displacements for a harmonic support motion function $w_s(t) = w_0\, e^{\imath\, \Omega_F t}$, with $w_0 = 0.001$m, and for various values of Ω_F. For each Ω_F, the steady state amplitudes are determined via convolution. After considering a number of different values for Ω_F, a set of frequency response diagram points is obtained and these are compared to the results obtained directly by analysing the FRF. If the proposed solution via the impulse response method and convolution yields the same results as the FRF analysis, it would provide another confirmation that the presented solution is valid.

For this analysis a system of 3 connected beams was considered. Each beam was of the same geometrical properties, relaxed elastic modulus and material mass density as described in the previous subsection, and the beam fractional order damping parameters adopted for this analysis were: $\alpha = 0.9$, $\tau_1^{\alpha} = 0.0002 s^{\alpha}$. The connecting layer stiffness, fractional derivative order and retardation time were taken to be $\kappa = 10000 \frac{N}{m^2}$, $\beta = 0.99$, $\tau_2^{\beta} = 0.0001 s^{\beta}$, respectively. The same total mass equal to the mass of a single beam was attached to each of the beams, but in different configurations. For the first beam the whole attached mass was positioned at the free end of the beam, for the second beam the total attached mass was divided equally into three parts and attached to the beam in the thirds of the span, while for the third beam the total mass was divided into two parts, one of which was attached to the beam midspan, and the other to the free end of the beam.

Fig. 3 shows the frequency response diagram for each of the three beams of the described system. The blue continuous line represents the graph of the frequency response function, while the red dotted line presents the interpolation between the frequency response diagram points obtained through convolution. As it can be seen from the figure, both the direct FRF solution and the solution with convolution presented in Section 3 yield very similar results. The difference becomes somewhat greater around the resonance state of the system, but the results are still in very good agreement. It can be observed that the convolution solution gives a bit larger displacement amplitudes than the ones obtained directly through FRF, which is to be expected since the off-diagonal elements of the "diagonalised" damping matrices were neglected in order to decouple the system equations. However, for a small damping case such as the one considered in this analysis, it is apparent that the error introduced by this approximation is relatively small and acceptable.

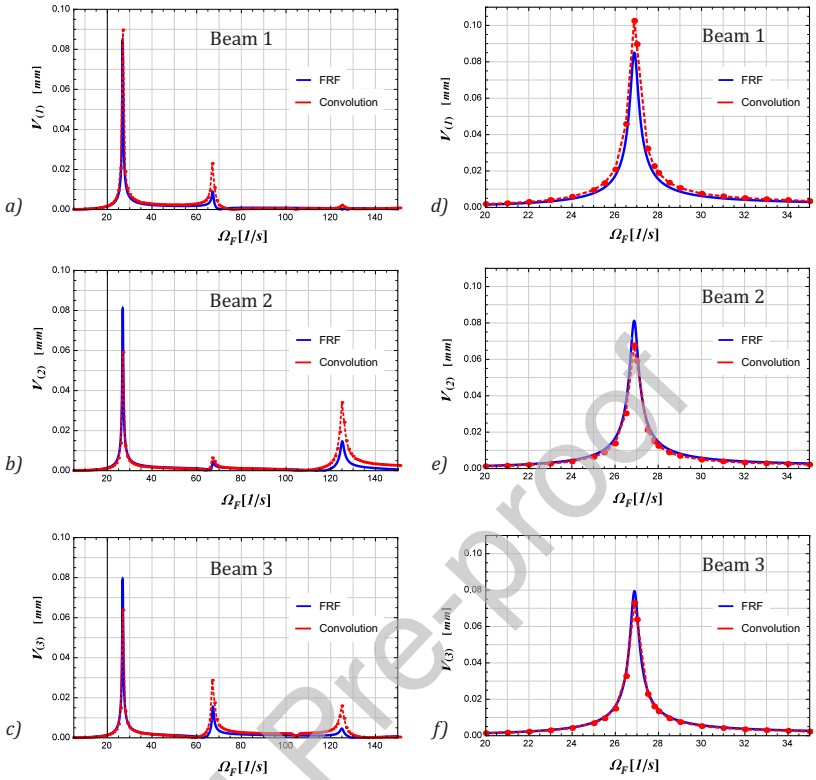

Figure 3: The frequency response diagram $v^{ss}_{(k)max}(L,\Omega)$ for the free end of each cantilever in the system of $N = 3$ connected beams with different number and position of the attached masses

6. Numerical studies

In this section, numerical investigation of the influence of the connecting layer properties, number of connected beams, number and position of the attached masses and properties of the connected beams themselves on the dynamic behaviour of the system are presented. First, the displacements and transient system behaviour will be analysed by using the solution presented in Section 3, under the same support motion function used for validation with FEM in Section 5.1. And after that, the analysis of influence of various system parameters on the system steady state response will be presented.

In all the subsequent analyses, geometrical characteristics of the connected beams are taken to be the same as in the validation section. However, the parameters such as number of beams N, number of concentrated masses $N_{m(k)}$ and their position $a_{(k)p}$, derivative order for the connecting layers β and their relaxed compliance coefficient κ, were all varied according to the particular analysis. The retardation time and the fractional derivative order for the *beam*

material constitutive equation and its influence on the system behaviour were not an object of the present study so they were fixed at the values of $\tau_1^\alpha = 0.002 s^\alpha$ and $\alpha = 0.9$ for all the numerical investigations. Again, only free beam chains were considered, with $\kappa_0 = \kappa_N = 0\ N/m^2$. Moreover, in all subsequent analyses, zero initial conditions were assumed.

6.1. *Transient analysis*

Influence of the order of fractional derivative of the connecting layer material

First, the influence of the order of the fractional derivative in the connecting layer material model on the dynamic behaviour of the system was investigated. A system of 3 beams, each carrying 2 attached masses of equal weight, was analysed. Values for the parameters describing the beam geometry and material model were adopted the same as described in the validation section. All the attached masses were equal to half of a single beam weight, and positioned at the free end and at the midspan of each beam. The relaxed compliance coefficient of the connecting layers was set to be $\kappa = 1000 N/m^2$, and the fractional derivative order in the constitutive equation for the layer material model was varied. The support motion function is taken the same as described in Section 5.

In Fig. 4 the relative displacements of the free end of the beams in the first 10 seconds of motion are presented, for the three representative cases: elastic layer - $\beta = 0$, layer with fractional-order damping - $\beta = 0.50$, and layer with an integer order viscous damping - $\beta = 1.00$.

As it can be seen from the Fig. 4, in the case of elastic connecting layer ($\beta = 0$) the vibrations are damped only due to internal damping in the beams ($\alpha = 0.9$), but they are attenuated more slowly compared to the cases with fractional viscoelastic connecting layers. And, as expected, the higher the derivative order for the layer material model is used, the higher the damping occurs in the system. It can be seen from the figure that the layer decreases the vibration amplitudes of the beams with the increase of fractional derivative order β.

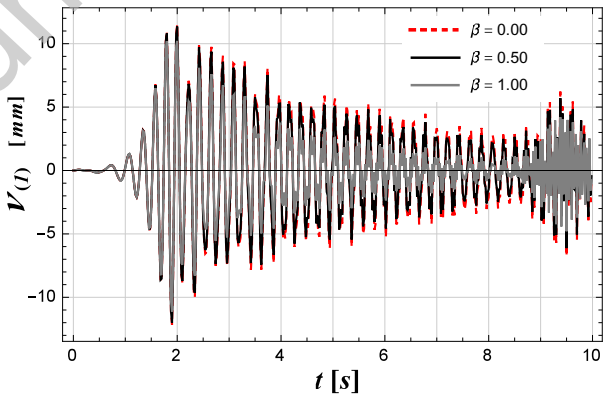

Figure 4: The relative displacements of the free end of the first beam $v_{(1)}(L,t)$ for various fractional derivative order in material model of the connecting layers

Influence of the position of the attached masses

Next, the influence of the position of attached concentrated masses on the dynamic behaviour of the system is investigated. For this purpose, a system with $N = 3$ connected beams, each carrying $N_{m(k)} = 2$ attached masses of half the single beam mass ($m_{(k)p} = 0.5, \quad p = 1, 2, \quad k = 1, 2, 3$), was analysed. Geometrical and material properties of all the beams are set to be the same, with the parameter values chosen as described in section 5. The connecting layers were modelled with the relaxed compliance coefficient of $\kappa = 200N/m^2$, retardation time $\tau_2^\beta = 0.001\, s^\beta$ and fractional derivative order of $\beta = 0.99$.

Two different positions of the attached masses in the system were considered - when all the beams carry one mass at the midspan and one at the free end, and when all the beams carry both attached masses at the free end.

The results of the analysis are presented in Fig. 5, which shows the relative displacements for all 3 beams of the system for both considered dispositions of the attached masses. Green line represents the beams with mass at the midspan and at the free end, while the red line represents displacements of beams with all the attached masses at the free end. In each mass disposition case, all the beams of the system have mutually equal displacements, since all the conditions, including the mass disposition, are identical.

It can be seen from the Fig. 5 that by positioning some of the attached mass at the midspan of the beams, the beams vibrate with larger amplitudes, which could potentially be used in some practical applications of this type of systems.

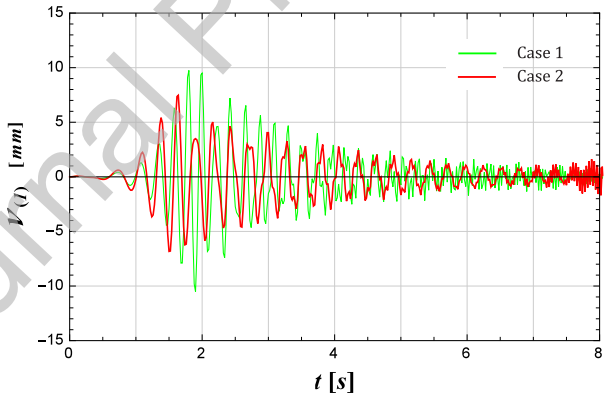

Figure 5: Relative displacements of the free end of the connected beams $v_{(k)}(L, t)$ for different positions of the attached masses; Case 1 - half of the added mass attached at the midspan, and the other half at the tip (green line), Case 2 - the whole added mass attached at the tip (red line)

Influence of the presence of "stiff core" in the system

The influence of different *beam* properties on the dynamic behaviour of the system is also analysed. To show how the presence of a beam with properties different from those of other beams in the system affects the system behaviour,

an array of 5 connected beams is analysed. Each beam is carrying 3 attached masses in the thirds of the span, and each mass equals one third of a single beam mass. Two different cases were considered. Case 1 - a system with all beams identical, and their geometrical and material properties set as described in Section 5. This system served as the reference case. Case 2 - a system identical to the one in the previous case, except that one of the beams has a three times greater cross-sectional moment of inertia and is therefore 3 times stiffer than the rest of the beams. This beam will be referred to as the "stiff core". In this case, the stiff core is positioned in the middle of the beam array, that is: $E_1I_1 = E_2I_2 = E_4I_4 = E_5I_5 = E_3I_3/3$. The connecting layer properties and the support motion function are taken to be the same as in the previous subsection.

The relative displacements of the free end of all the beams in the system are presented in Fig. 6.

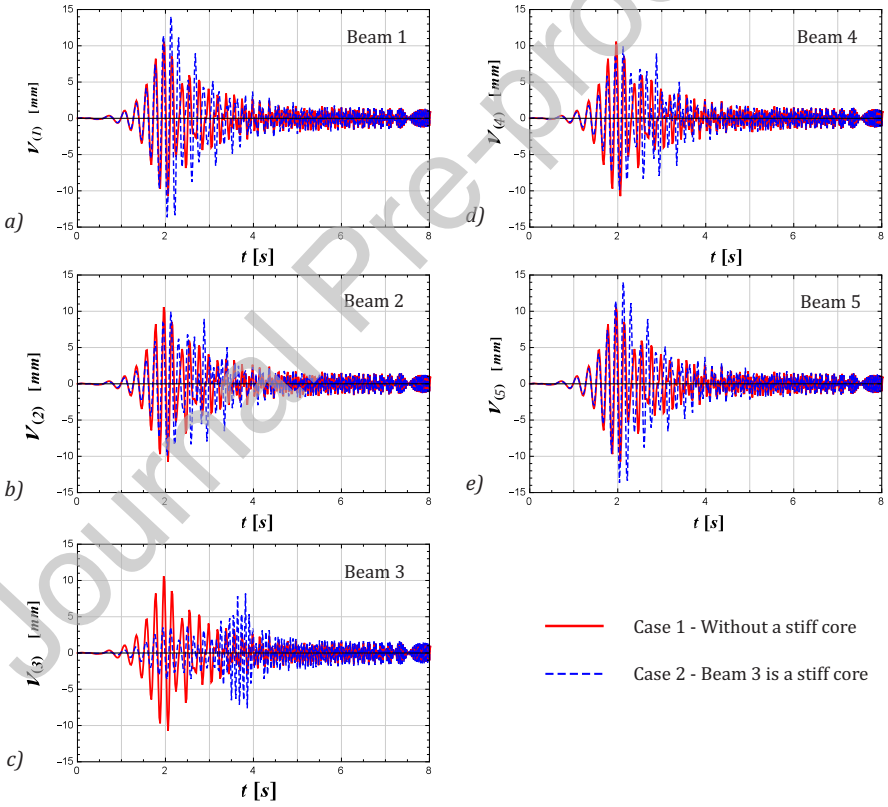

Figure 6: The relative displacements of the free end of 5 connected beams $v_{(k)}(L,t)$ for different positions of the stiff core

It can be seen from figure that in the case without a stiff core (red, continuous lines) all the beams have the same displacements since the vibration conditions

are identical. On the other hand, if the stiff core is put in the middle of the beam chain (blue, dashed lines), vibration amplitudes of the connected beams are mutually different. It can be seen that the amplitudes of the beams that are farthest from the core are the highest, while the middle beam that acts as the stiff core for the system has the lowest amplitudes.

Thus the stiff core obviously affects the dynamic behaviour of the system, but, perhaps somewhat counterintuitively, its presence leads to overall higher vibration amplitudes of the connected beams. This phenomenon should be investigated further, but that analysis transcends the scope of this paper.

6.2. Steady state response analysis

The previous numerical studies were done by using the solution for beam displacements as a function of time, presented in Section 3. However, a useful insight into the system behaviour can also be obtained by analysing the system response in a steady state vibration regime. If a system arrives at a steady state, its behaviour depends on the frequency of the present harmonic excitation (e.g. [7, 60]), so it can be most conveniently described by the frequency response diagram. In the following analyses, the influence of several parameters on the system steady state behaviour will be investigated, by first determining the frequency response function (FRF) for each considered case as described in Section 4, and then using this function to graph the required frequency response diagrams. In all the analyses, the support motion function was taken to be a harmonic function as described in Section 4, with the amplitude of $w_0 = 0.001m$.

Influence of the connecting layers relaxed compliance coefficient

First, the influence of the connecting layers relaxed compliance coefficient on the system steady state behaviour was investigated. For this analysis, a system of 3 beams of the same geometrical and material properties as in validation section was considered. One concentrated mass was attached to the free end of each beam. If the mass of a single beam is denoted with m_B, then the masses attached to the first, second and third beam weighted $1.0m_B$, $0.6m_B$ and $0.3m_B$, respectively. Fig. 7 shows the frequency response diagrams for different values of the layers' coefficient.

Three different cases were considered. First, the compliance coefficient was set to be equal to zero, that is, the beams were treated as disconnected and they vibrated separately. In the next two cases the compliance coefficient was set to be $\kappa = 100\frac{N}{m^2}$ and $\kappa = 300\frac{N}{m^2}$, respectively, and the results for all three beams and all three cases are shown in Fig. 7.

Several facts can be observed in Fig. 7.

First, if the beams are not connected (i.e. $\kappa = 0$, blue lines in Fig. 7), in the considered frequency range there is only one resonance state for each of the three beams represented by a single peak in the frequency response diagram, and no influence is transferred between the beams. The resonance occurs when the excitation frequency approaches the natural frequency of the beam, and it can be seen that the base natural frequency for each of the three considered

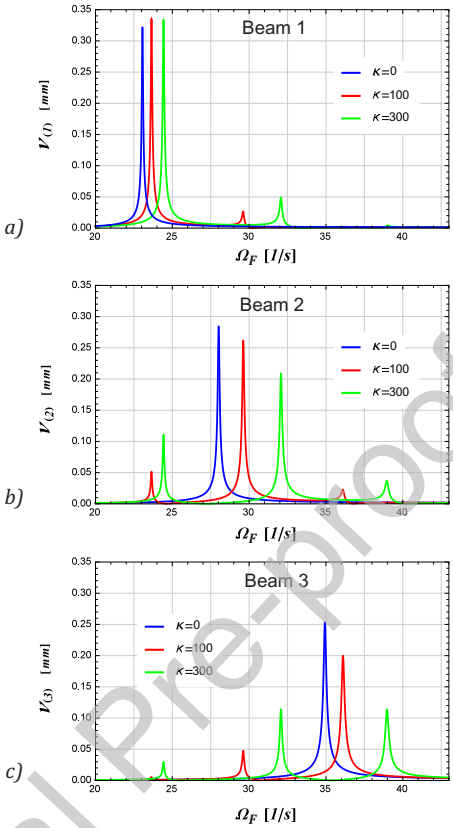

Figure 7: The frequency response diagrams of the 3 connected beams for different values of the connecting layer relaxed compliance coefficient κ

beams is different - the larger the mass attached to the tip of the beam, the lower the base natural frequency of the beam.

Next, in both cases with connected beams (red and green lines in Fig. 7), it can be seen that for each of the beams there are 3 large-amplitude vibration states, since the vibrations are transferred through the system due to the presence of the connecting layer. For instance, if the case with $\kappa = 300\frac{N}{m^2}$ is observed (green lines), it can be seen that the first beam enters a resonance for excitation frequency around $24.5\,s^{-1}$, which is the natural frequency of that beam. For the same excitation frequency, now the second and the third beam also experience larger amplitudes. This happens because vibration energy from the first beam gets transferred to the second, and afterwards to the third beam. However, the amplitudes of the first beam in the first resonant state of the system are much larger than those of the second and the third beam, since this is the natural frequency of the first beam so the first system resonance originates from it. On the other hand, for excitation frequency of around $32.2\,s^{-1}$, the

system also enters the resonant state, but this time due to the resonance of the second beam. This time, the resonance is most pronounced on the second beam, and the amplitudes of the first and the third beam are considerably lower. Similar effect can be observed around the excitation frequency of 39.1 s^{-1}, when the third beam enters its resonant state. However, since the mass attached to the third beam is much smaller than the one attached to the first beam, it can be seen that the third beam resonance has little effect on the second, and almost no effect on the first beam. The same phenomenon as the one just described is observed for a case with lower relaxed compliance coefficient ($\kappa = 100\frac{N}{m^2}$, red lines in Fig. 7), but since the connecting layer stiffness is lower, so the amplitudes are lower.

Another observation is that the connecting layers compliance coefficient affects the values of natural frequencies of the system. And as expected, the higher the coefficient, the higher the system natural frequencies. Consequently, as it can be seen in Fig. 7, the frequency response diagram (or, more precisely, the resonant states of the system) gets shifted to the right as the value of relaxed compliance coefficient increases.

Influence of the number and position of the attached masses

Next, the influence of the number, position and distribution of the attached masses was investigated. For this analysis, a system of three connected beams of the same geometrical and material properties as described in the validation section was studied. The connecting layer relaxed compliance coefficient was set to be $\kappa = 300\frac{N}{m^2}$. Again, if the mass of a single beam is denoted with m_B, then the total mass attached to the first, second and third beam was $1.0\,m_B$, $0.8\,m_B$ and $0.6\,m_B$, respectively, but this total attached mass was distributed in three different ways. In the first case, Case 1, all the attached mass was concentrated at the free end for all the beams. In Case 2, half of the total attached mass was positioned at the midspan of each beam, and the other half at the free end. In Case 3, the total attached mass was distributed differently in each beam of the system - for the first beam, all the attached mass of $1.0\,m_B$ was attached to the free end, on the second beam, one half of the total attached mass of $0.8\,m_B$ was attached at the midspan and the other at the free end of the beam, and for the third beam, the total attached mass of $0.6\,m_B$ was divided equally into three parts and attached in thirds of the beam span. The results for all three beams and all three considered cases of the attached mass distribution are shown in Fig. 8.

Again, there are several observations that can be made when considering Fig. 8. For instance, for the first two considered cases - that is, with the whole attached mass concentrated at the free end (blue lines) and with the total attached mass equally divided and positioned at the midspan and at the free end of the beams (red lines) - it can be seen that the frequency response is practically the same, only shifted for a certain amount. As expected, if the whole attached mass is located at the free end, the system natural frequencies are lower, but the amplitudes are very similar, even in the resonant states.

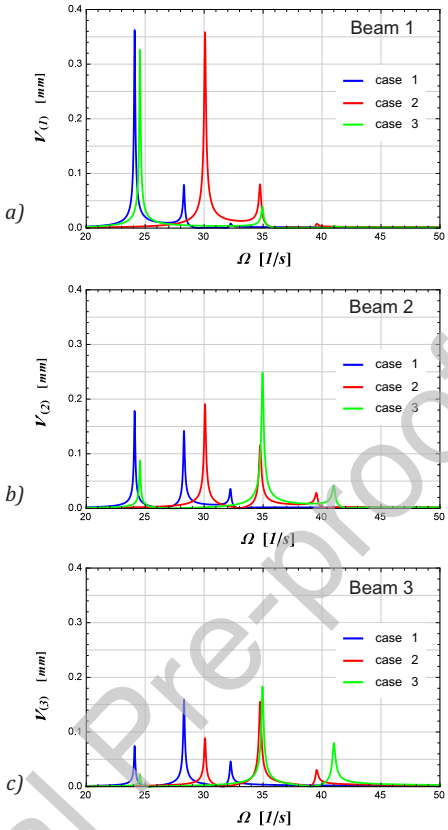

Figure 8: The frequency response diagrams of the 3 connected beams for different distributions of the total attached mass; Case 1 - whole attached mass concentrated at the free end in all three beams, Case 2 - half the attached mass at the midspan, half at the free end in all three beams, Case 3 - different attached mass distribution in all three beams

Another interesting observation that follows from Fig. 8 is that by the appropriate distribution and positioning of the attached mass, the steady state response of the system *can be tailored at will*, according to the particular needs for any given system. Namely, in all three considered cases, the same total mass was added to the system, and it was only distributed differently, but the behaviour of the system was changed dramatically. For instance, not only that the resonant frequency range for the whole system can be shifted by changing the balance of the attached masses (e.g. as in Cases 1 and 2), thus changing all the natural frequencies of the system for the same amount, but with the appropriate distribution of the attached masses *each individual natural frequency of the system can be changed at will*. Example of this can be seen in Fig. 8. In Case 3 (green lines), the first natural frequency of the system is almost the same as in Case 1. However, the second natural frequency was shifted higher and it is

almost the same as the first natural frequency of Case 2. In this way, the second resonant state occurring in Case 1, and the first resonant state occurring in Case 2 are avoided, and only the desired resonant states of the system are kept. This opens a wide range of possibilities for the design of systems of connected beams and their practical application.

Influence of the number of beams

Finally, the influence of the number of connected beams on the system steady state behaviour was investigated. For this analysis, 4 beams of the same geometrical and material properties as in previous section were analysed, each carrying one concentrated mass attached at the free end. As before, if the mass of a single beam is denoted with m_B, then the total mass attached to the first, second, third and fourth beam was $1.0\,m_B$, $0.8\,m_B$, $0.6\,m_B$ and $0.4\,m_B$, respectively. Two different cases were considered. First, only the first two and the second two beams were mutually connected by a connecting layer, with coefficient $\kappa = 300\frac{N}{m^2}$, while there was no connection between the second and the third beam in the chain. So, there were effectively two independent systems, each consisting of two connected beams. In the other case, the connection was added between the second and the third beam so all the beams were integrated into a single system. All the results are shown in Fig. 9. Blue lines represent the frequency responses for the first two beams when there is no connection between them and the other two beams, and red lines present the frequency response diagrams for the second two beams in the same case. Green lines present the frequency responses of each beam when all four beams are connected into a single system.

As it can be seen from the Fig. 9, when there are two pairs of connected beams (blue and red lines), each beam exhibits two large-amplitude vibration states - one originating from entering its own resonant state, and one induced by the resonance of another beam it's connected to. On the other hand, when all four beams are connected (green lines), each beam exhibits four large-amplitude states, one as a consequence of its own resonance, and three induced by other beams' resonant states. As in the previous analysis, the induced resonances are less pronounced, and even more so as the beam in which the particular system resonance originates is farther from the considered beam. Again, the induced resonance amplitudes depend largely on the connecting layer properties.

Nevertheless, it can be seen that by increasing the number of connected beams, more influence is transferred between the beams and each beam experiences more large-amplitude states, while the size of these large amplitudes can be modified by tuning the connecting layer properties. This in turn means that, from a possible energy harvesting point of view, each beam has a broader operational range than it would have had if it was isolated. Namely, systems of the type considered in this paper can be applied for energy harvesting purposes if, for instance, piezoelectric elements are added between the beams, or if the beams themselves are made as bimorph beams with piezoceramic layers on one side or both sides (as presented in [6] for example). This means that the beams' deformation is directly proportional to the expected electrical energy output.

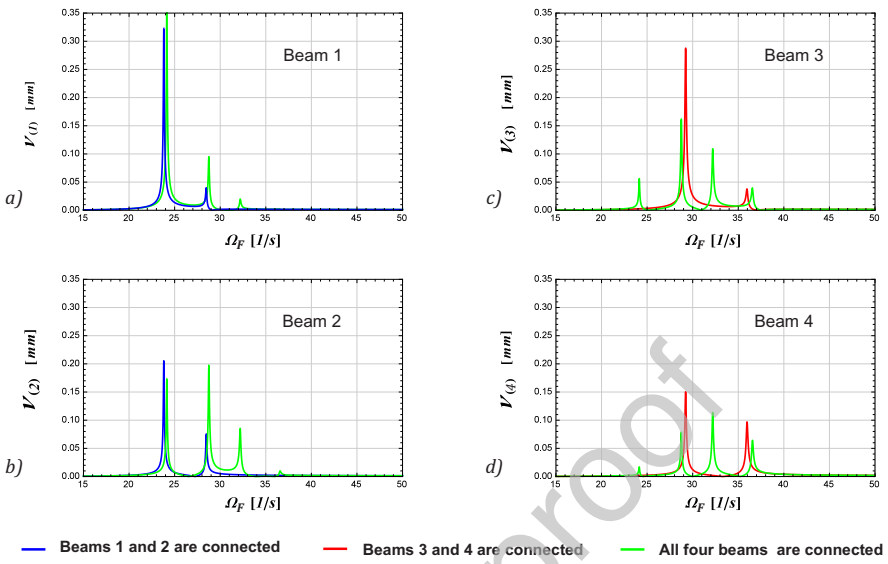

Figure 9: The frequency response diagrams of 4 connected beams with various connection configurations and various masses attached to their free end

Therefore, if the beams are connected, since then each beam experiences large amplitude vibrations for more different values of the excitation frequency, the operational range of such energy harvesting device becomes wider. Moreover, this operational range can be tuned at will, in accordance with particular needs for a given problem, by the appropriate system configuration, that is, by using the optimal number of adequately connected beams with the appropriate mass distribution throughout the system, and the model presented in this paper can be used as a tool for finding the optimum parameter values of such systems.

Additionally, as previously shown, the frequency response of the system can also be modified by different attached mass distribution and material properties of the beams. This could also be used for intentionally increasing the vibration amplitudes and improve the efficiency of the energy harvesting system based on the multi-beam model discussed herein. It should also be pointed out that, as it was mentioned in the introductory section, commonly up to three concentrated masses are attached to beams in energy harvesting systems to improve their performance. Hence, in this paper, only systems with one, two or three attached masses are considered. However, the model presented herein gives the ability to examine the influence of any mass number and disposition on the dynamic behaviour of the system, and makes it possible to find the optimal mass disposition that would produce the desired values of output parameters.

7. Concluding remarks

In the presented paper the problem of transversal vibrations of a system of arbitrary number of connected Euler-Bernoulli cantilever beams, each carrying an arbitrary number of attached concentrated masses, subjected to arbitrary motion of their supports is investigated. Masses can be of arbitrary weight and any position on the beams. Beams can have various geometrical characteristics and fractional viscoelastic properties modelled by using a Kelvin-Voigt type fractional-order constitutive equation of the same, yet arbitrary order. The beams are connected by fractional viscoelastic layers of constant properties throughout the system, and also modelled by a Kelvin-Voigt type fractional order force-displacement relation.

The solution is sought through applying the Galerkin analytical approximate method to deal with the influence of the attached masses on the orthogonality conditions, and the Fourier transform to solve the system of coupled fractional order differential equations, assuming that the system damping is relatively small. First the impulse system response is determined by analysing the Green functions, and then the convolution between them and the inertial forces is taken in order to obtain the total system response.

The steady state behaviour of the system is also analysed and the expressions for the frequency response functions are derived.

The model is validated by the Finite Element Method for a special case with elastic beams and integer order derivative constitutive equation for the connecting layer material, and also for the steady state vibration regime by comparing the convolution results with the frequency response function values.

The influence of various parameters such as the number of the connected beams, the order of fractional derivative in the connecting layer material model, the position of the attached masses and the presence of beams with different elastic properties on the dynamic behaviour of the system is investigated, both in transient and in the steady state vibration regime. Numerical studies revealed several phenomena that could potentially be applied in the analysis and the design process of energy harvesting systems consisting of multiple connected beams.

The presented model is developed for the case with relatively small general damping present in the system. Therefore, it should be further developed to include other damping cases, as well as different material properties of beams and connecting layers in the system. Also, the model could be extended with a higher-order beam theory and accounting for nonlinear effects. However, the solution and analysis methodology proposed in this paper present a solid and useful starting point in analysis of systems of connected beams with attached masses under base excitation and their application in energy harvesting or composite material modelling.

Acknowledgements

This research was supported by the Ministry of Education, Science and Technology of the Republic of Serbia, through the Mathematical Institute SANU, Belgrade, and the Grant No. 174001, and the author D. Karličić was supported by the Marie SkÅĆodowska-Curie Actions - European Commission fellowship: 799201-METACTIVE.

References

[1] Abha Misra, Jordan R Raney, Luigi De Nardo, Anna E Craig, and Chiara Daraio. Synthesis and characterization of carbon nanotube–polymer multilayer structures. *Acs Nano*, 5(10):7713–7721, 2011.

[2] A Ghorbanpour Arani, H BabaAkbar Zarei, M Eskandari, and P Pourmousa. Vibration behavior of visco-elastically coupled sandwich beams with magnetorheological core and three-phase carbon nanotubes/fiber/polymer composite facesheets subjected to external magnetic field. *Journal of Sandwich Structures & Materials*, page 1099636217743177, 2017.

[3] Allan Manalo, Thiru Aravinthan, Amir Fam, and Brahim Benmokrane. State-of-the-art review on frp sandwich systems for lightweight civil infrastructure. *Journal of Composites for Construction*, 21(1):04016068, 2016.

[4] Victor Birman and George A Kardomateas. Review of current trends in research and applications of sandwich structures. *Composites Part B: Engineering*, 142:221–240, 2018.

[5] Yan Cui, Qunying Zhang, Minglei Yao, Weijie Dong, and Shiqiao Gao. Vibration piezoelectric energy harvester with multi-beam. *Aip Advances*, 5(4):041332, 2015.

[6] Viviana Meruane and K Pichara. A broadband vibration-based energy harvester using an array of piezoelectric beams connected by springs. *Shock and Vibration*, 2016, 2016.

[7] Shengxi Zhou, Bo Yan, and Daniel Inman. A novel nonlinear piezoelectric energy harvesting system based on linear-element coupling: design, modeling and dynamic analysis. *Sensors*, 18(5):1492, 2018.

[8] Max-Uwe Noll, Lukas Lentz, and Utz von Wagner. On the discretization of a bistable cantilever beam with application to energy harvesting. *Facta Universitatis, Series: Mechanical Engineering*, 17(2):125–139, 2019.

[9] Paul Cahill, Budhaditya Hazra, Raid Karoumi, Alan Mathewson, and Vikram Pakrashi. Vibration energy harvesting based monitoring of an operational bridge undergoing forced vibration and train passage. *Mechanical Systems and Signal Processing*, 106:265–283, 2018.

[10] Jiayu Chen, Qiwen Qiu, Yilong Han, and Denvid Lau. Piezoelectric materials for sustainable building structures: Fundamentals and applications. *Renewable and Sustainable Energy Reviews*, 101:14–25, 2019.

[11] Zhiwei Zhang, Hongjun Xiang, Zhifei Shi, and Jiawang Zhan. Experimental investigation on piezoelectric energy harvesting from vehicle-bridge coupling vibration. *Energy conversion and management*, 163:169–179, 2018.

[12] H. Wang, A. Jasim, and X. Chen. Energy harvesting technologies in roadway and bridge for different applicationsâĂŞa comprehensive review. *Applied energy*, 212(1):1083–1094, 2018.

[13] Zhengbao Yang, Shengxi Zhou, Jean Zu, and Daniel Inman. High-performance piezoelectric energy harvesters and their applications. *Joule*, 2(4):642–697, 2018.

[14] JM Seelig, II Hoppmann, et al. Impact on an elastically connected double beam system. Technical report, RENSSELAER POLYTECHNIC INST TROY NY, 1963.

[15] JM Seelig and WH Hoppmann. Normal mode vibrations of systems of elastically connected parallel bars. *The Journal of the Acoustical Society of America*, 36(1):93–99, 1964.

[16] PG Kessel. Resonances excited in an elastically connected double-beam system by a cyclic moving load. *The Journal of the Acoustical Society of America*, 40(3):684–687, 1966.

[17] PG Kessel and TF Raske. Damped response of an elastically connected double-beam system due to a cyclic moving load. *The Journal of the Acoustical Society of America*, 42(4):873–881, 1967.

[18] Singiresu S Rao. Natural vibrations of systems of elastically connected timoshenko beams. *The Journal of the Acoustical Society of America*, 55(6):1232–1237, 1974.

[19] Z. Oniszczuk. Free transverse vibrations of an elastically connected double-beam system. *Journal of Theoretical and Applied Mechanics*, 3(1):162–171, 1976.

[20] Tadataka R Hamada, Hidetaro NAKAYAMA, and Kunio HAYASHI. Free and forced vibrations of elastically connected double-beam systems. *Bulletin of JSME*, 26(221):1936–1942, 1983.

[21] Stanisław Kukla and Bogdan Skalmierski. Free vibration of a system composed of two beams separated by an elastic layer. *Journal of Theoretical and Applied Mechanics*, 32(3):581–590, 1994.

[22] HV Vu, AM Ordonez, and BH Karnopp. Vibration of a double-beam system. *Journal of sound and vibration*, 229(4):807–822, 2000.

[23] Z Oniszczuk. Free transverse vibrations of elastically connected simply supported double-beam complex system. *Journal of sound and vibration*, 232(2):387–403, 2000.

[24] Jun Li, Yong Chen, and Hongxing Hua. Exact dynamic stiffness matrix of a timoshenko three-beam system. *International Journal of Mechanical Sciences*, 50(6):1023–1034, 2008.

[25] Z Oniszczuk. Forced transverse vibrations of an elastically connected complex simply supported double-beam system. *Journal of Sound and Vibration*, 264(2):273–286, 2003.

[26] S Graham Kelly and Shirish Srinivas. Free vibrations of elastically connected stretched beams. *Journal of Sound and Vibration*, 326(3-5):883–893, 2009.

[27] S Graham Kelly. Free and forced vibrations of elastically connected structures. *Advances in Acoustics and Vibration*, 2010, 2010.

[28] S Graham Kelly. *Advanced vibration analysis*. CRC Press, 2006.

[29] WKF Brito, CDCD Maia, and AV Mendonça. Bending analysis of elastically connected euler-bernoulli double-beam system using the direct boundary element method. *Applied Mathematical Modelling*, 2019.

[30] Michael Dublin. Forced responses of two elastic beams interconnected by spring-damper systems. *Journal of the Aeronautical Sciences*, 23(9):824–829, 1956.

[31] S Graham Kelly and Clint Nicely. Free vibrations of a series of beams connected by viscoelastic layers. *Advances in Acoustics and Vibration*, 2015, 2015.

[32] Katica Stevanović Hedrih. Dynamics of coupled systems. *Nonlinear Analysis: Hybrid Systems*, 2(2):310–334, 2008.

[33] Danilo Karličić, Tony Murmu, Milan Cajić, Predrag Kozić, and Sondipon Adhikari. Dynamics of multiple viscoelastic carbon nanotube based nanocomposites with axial magnetic field. *Journal of Applied Physics*, 115(23):234303, 2014.

[34] Danilo Karličić, Predrag Kozić, and Ratko Pavlović. Nonlocal vibration and stability of a multiple-nanobeam system coupled by the winkler elastic medium. *Applied Mathematical Modelling*, 40(2):1599–1614, 2016.

[35] Z. Oniszczuk. Free transverse vibrations of an elastically connected double-beam system with concentrated masses, elastic and rigid supports (in polish). *Journal of Theoretical and Applied Mechanics*, 16(1):236–250, 1989.

[36] MN Hamdan and L Abdel Latif. On the numerical convergence of discretization methods for the free vibrations of beams with attached inertia elements. *Journal of sound and vibration*, 169(4):527–545, 1994.

[37] KH Low. On the methods to derive frequency equations of beams carrying multiple masses. *International Journal of Mechanical Sciences*, 43(3):871–881, 2001.

[38] Giuseppe Failla. An exact modal analysis approach to vibration analysis of structures with mass-spring subsystems and rotational joints. *Journal of Sound and Vibration*, 438:191–219, 2019.

[39] CWS To. Vibration of a cantilever beam with a base excitation and tip mass. *Journal of Sound and Vibration*, 83(4):445–460, 1982.

[40] E Esmailzadeh and G Nakhaie-Jazar. Periodic behavior of a cantilever beam with end mass subjected to harmonic base excitation. *International journal of non-linear mechanics*, 33(4):567–577, 1998.

[41] Wang Hongjin, Meng Qingfeng, and Feng Wuwei. Discussion of the improved methods for analyzing a cantilever beam carrying a tip-mass under base excitation. *Shock and Vibration*, 2014, 2014.

[42] Vamsi C Meesala and Muhammad R Hajj. Parameter sensitivity of cantilever beam with tip mass to parametric excitation. *Nonlinear Dynamics*, pages 1–10, 2019.

[43] Alper Erturk and Daniel J Inman. *Piezoelectric energy harvesting*. John Wiley & Sons, 2011.

[44] Yuriy A Rossikhin and Marina V Shitikova. Application of fractional calculus for dynamic problems of solid mechanics: novel trends and recent results. *Applied Mechanics Reviews*, 63(1):010801, 2010.

[45] Siegmar Kempfle, Ingo Schäfer, and Horst Beyer. Fractional calculus via functional calculus: theory and applications. *Nonlinear Dynamics*, 29(1-4):99–127, 2002.

[46] Ingo Schäfer and Siegmar Kempfle. Impulse responses of fractional damped systems. *Nonlinear Dynamics*, 38(1-4):61–68, 2004.

[47] Jan Freundlich. Vibrations of a simply supported beam with a fractional viscoelastic material model–supports movement excitation. *Shock and Vibration*, 20(6):1103–1112, 2013.

[48] Jan Freundlich. Transient vibrations of a fractional kelvin-voigt viscoelastic cantilever beam with a tip mass and subjected to a base excitation. *Journal of Sound and Vibration*, 438:99–115, 2019.

[49] Paweł Łabędzki, Rafał Pawlikowski, and Andrzej Radowicz. Transverse vibration of a cantilever beam under base excitation using fractional rheological model. In *AIP Conference Proceedings*, volume 2029, page 020034. AIP Publishing, 2018.

[50] Milan Cajic, Danilo Karlicic, and Mihailo Lazarevic. Nonlocal vibration of a fractional order viscoelastic nanobeam with attached nanoparticle. *Theoretical and Applied Mechanics*, 42(3):167–190, 2015.

[51] Milan Cajić, Mihailo Lazarević, Danilo Karličić, HongGuang Sun, and Xiaoting Liu. Fractional-order model for the vibration of a nanobeam influenced by an axial magnetic field and attached nanoparticles. *Acta Mechanica*, 229(12):4791–4815, 2018.

[52] Olga Martin. Nonlocal effects on the dynamic analysis of a viscoelastic nanobeam using a fractional zener model. *Applied Mathematical Modelling*, 73:637–650, 2019.

[53] I Podlubny and Martin Kacenak. Isoclinal matrices and numerical solution of fractional differential equations. In *2001 European Control Conference (ECC)*, pages 1467–1470. IEEE, 2001.

[54] AC Galucio, JF Deu, and R Ohayon. A fractional derivative viscoelastic model for hybrid active-passive damping treatments in time domain-application to sandwich beams. *Journal of Intelligent Material Systems and Structures*, 16(1):33–45, 2005.

[55] Stepa Paunović, Milan Cajić, Danilo Karlićić, and Marina Mijalković. A novel approach for vibration analysis of fractional viscoelastic beams with attached masses and base excitation. *Journal of Sound and Vibration*, page 114955, 2019.

[56] Singiresu S Rao. *Vibration of continuous systems*, volume 464. Wiley Online Library, 2007.

[57] Leonard Meirovitch. *Elements of vibration analysis*. McGraw-Hill Science, Engineering & Mathematics, 1975.

[58] Yu A Rossikhin, Marina V Shitikova, and TA Shcheglova. Analysis of free vibrations of a viscoelastic oscillator via the models involving several fractional parameters and relaxation/retardation times. *Computers & Mathematics with Applications*, 59(5):1727–1744, 2010.

[59] Yuriy A Rossikhin and Marina V Shitikova. New approach for the analysis of damped vibrations of fractional oscillators. *Shock and Vibration*, 16(4):365–387, 2009.

[60] Alper Erturk and Daniel J Inman. An experimentally validated bimorph cantilever model for piezoelectric energy harvesting from base excitations. *Smart materials and structures*, 18(2):025009, 2009.

Appendix 1: Elements of the matrices and vectors for the (k)-th beam in the Galerkin approximation

$$\left[\mathbf{K}_{(k)_{k-1}}\right]_{ij} = -\kappa_{(k-1)} \int_0^L \phi_{(k-1)i}\phi_{(k)j}dx = \begin{cases} -\frac{\kappa_{(k-1)}}{\sqrt{\rho_{k-1}A_{k-1}}\sqrt{\rho_k A_k}} & \text{for } i=j \\ 0 & \text{for } i\neq j \end{cases}$$

$$\left[\mathbf{K}_{(k)_k}\right]_{ij} = \int_0^L E_k I_k \phi''''_{(k)i}(x)\phi_{(k)j}(x)dx + (\kappa_{(k)}+\kappa_{(k-1)}) \int_0^L \phi_{(k)i}\phi_{(k)j}dx =$$
$$= \begin{cases} \bar{\omega}^2_{(k)i} + \frac{(\kappa_{(k)}+\kappa_{(k-1)})}{\rho_k A_k} & \text{for } i=j \\ 0 & \text{for } i\neq j \end{cases}$$

$$\left[\mathbf{K}_{(k)_{k+1}}\right]_{ij} = -\kappa_{(k)} \int_0^L \phi_{(k-1)i}\phi_{(k)j}dx = \begin{cases} -\frac{\kappa_{(k)}}{\sqrt{\rho_k A_k}\sqrt{\rho_{k+1}A_{k+1}}} & \text{for } i=j \\ 0 & \text{for } i\neq j \end{cases}$$

$$\left[\mathbf{C}_{\alpha(k)_k}\right]_{ij} = \tau_1^\alpha \int_0^L E_k I_k \phi''''_{(k)i}(x)\phi_{(k)j}(x)dx = \begin{cases} \tau_1^\alpha \bar{\omega}^2_{(k)i} & \text{for } i=j \\ 0 & \text{for } i\neq j \end{cases}$$

$$\left[\mathbf{C}_{\beta(k)_{k-1}}\right]_{ij} = -\tau_2^\beta \kappa_{(k-1)} \int_0^L \phi_{(k-1)i}\phi_{(k)j}dx = \begin{cases} -\tau_2^\beta \frac{\kappa_{(k-1)}}{\sqrt{\rho_{k-1}A_{k-1}}\sqrt{\rho_k A_k}} & \text{for } i=j \\ 0 & \text{for } i\neq j \end{cases}$$

$$\left[\mathbf{C}_{\beta(k)_k}\right]_{ij} = \tau_2^\beta (\kappa_{(k)}+\kappa_{(k-1)}) \int_0^L \phi_{(k)i}\phi_{(k)j}dx = \begin{cases} \tau_2^\beta \frac{(\kappa_{(k)}+\kappa_{(k-1)})}{\rho_k A_k} & \text{for } i=j \\ 0 & \text{for } i\neq j \end{cases}$$

$$\left[\mathbf{C}_{\beta(k)_{k+1}}\right]_{ij} = -\tau_2^\beta \kappa_k \int_0^L \phi_{(k+1)i}\phi_{(k)j}dx = \begin{cases} -\tau_2^\beta \frac{\kappa_{(k)}}{\sqrt{\rho_k A_k}\sqrt{\rho_{k+1}A_{k+1}}} & \text{for } i=j \\ 0 & \text{for } i\neq j \end{cases}$$

$$\left[\mathbf{M}_{(k)_k}\right]_{ij} = \int_0^L \left(\rho_k A_k + \sum_{p=1}^{N_{m(k)}} m_{(k)p}\delta(x-a_{(k)p})\right) \phi_{(k)i}(x)\phi_{(k)j}(x)dx =$$
$$= \begin{cases} 1+\sum_{p=1}^{N_{m(k)}} m_{(k)p}\phi^2_{(k)i}(a_{(k)p}) & \text{for } i=j \\ \sum_{p=1}^{N_{mk}} m_{(k)p}\phi_{(k)i}(a_{(k)p})\phi_{(k)j}(a_{(k)p}) & \text{for } i\neq j \end{cases}$$

$$\left\{\mathbf{Q}_k\right\}_j = Q_{(k)_j}(t) = \int_0^L F_{(k)}(x,t)\phi_{(k)j}(x)dx$$

$$\left\{\mathbf{q}_k\right\}_j = q_{(k)_j}(t) \quad \Leftrightarrow \quad \mathbf{q}_k^T = [q_{(k)_1}, q_{(k)_2}, ..., q_{(k)_n}]$$

$$i = 1,2,\ldots,n\,; \quad j = 1,2,\ldots,n$$

Appendix 2: Matrix equation for the whole system

With the notation introduced in (16), and with the matrix elements for (k)-th beam defined in Appendix 1, the matrix for the whole system of N beams can be represented as:

$$
\begin{bmatrix}
\begin{bmatrix}\mathbf{K}_{(1)_1}\\ \mathbf{K}_{(2)_1}\end{bmatrix} & \begin{bmatrix}\mathbf{K}_{(1)_2}\\ \mathbf{K}_{(2)_2}\\ \mathbf{K}_{(3)_2}\end{bmatrix} & \begin{bmatrix}\mathbf{K}_{(2)_3}\\ \mathbf{K}_{(3)_3}\end{bmatrix} & \begin{bmatrix}\mathbf{K}_{(3)_4}\end{bmatrix} & & & \\
& & & \ddots & & & \\
& & & \begin{bmatrix}\mathbf{K}_{(N-1)_{N-2}}\end{bmatrix} & \begin{bmatrix}\mathbf{K}_{(N-1)_{N-1}}\\ \mathbf{K}_{(N)_{N-1}}\end{bmatrix} & \begin{bmatrix}\mathbf{K}_{(N-1)_N}\\ \mathbf{K}_{(N)_N}\end{bmatrix}
\end{bmatrix}
\begin{Bmatrix}\mathbf{q}_1\\ \mathbf{q}_2\\ \mathbf{q}_3\\ \mathbf{q}_4\\ \vdots\\ \mathbf{q}_{n\cdot N-1}\\ \mathbf{q}_{n\cdot N}\end{Bmatrix} +
$$

$$
\begin{bmatrix}
\begin{bmatrix}\mathbf{C}_{\alpha(1)_1}\end{bmatrix} & & & & & \\
& \begin{bmatrix}\mathbf{C}_{\alpha(2)_2}\end{bmatrix} & & & & \\
& & \begin{bmatrix}\mathbf{C}_{\alpha(3)_3}\end{bmatrix} & & & \\
& & & \ddots & & \\
& & & & \begin{bmatrix}\mathbf{C}_{\alpha(N-1)_{N-1}}\end{bmatrix} & \\
& & & & & \begin{bmatrix}\mathbf{C}_{\alpha(N)_N}\end{bmatrix}
\end{bmatrix}
D^{\alpha}
\begin{Bmatrix}\mathbf{q}_1\\ \mathbf{q}_2\\ \mathbf{q}_3\\ \mathbf{q}_4\\ \vdots\\ \mathbf{q}_{n\cdot N-1}\\ \mathbf{q}_{n\cdot N}\end{Bmatrix} +
$$

$$
\begin{bmatrix}
\begin{bmatrix}\mathbf{C}_{\beta(1)_1}\\ \mathbf{C}_{\beta(2)_1}\end{bmatrix} & \begin{bmatrix}\mathbf{C}_{\beta(1)_2}\\ \mathbf{C}_{\beta(2)_2}\\ \mathbf{C}_{\beta(3)_2}\end{bmatrix} & \begin{bmatrix}\mathbf{C}_{\beta(2)_3}\\ \mathbf{C}_{\beta(3)_3}\end{bmatrix} & \begin{bmatrix}\mathbf{C}_{\beta(3)_4}\end{bmatrix} & & & \\
& & & \ddots & & & \\
& & & \begin{bmatrix}\mathbf{C}_{\beta(N-1)_{N-2}}\end{bmatrix} & \begin{bmatrix}\mathbf{C}_{\beta(N-1)_{N-1}}\\ \mathbf{C}_{\beta(N)_{N-1}}\end{bmatrix} & \begin{bmatrix}\mathbf{C}_{\beta(N-1)_N}\\ \mathbf{C}_{\beta(N)_N}\end{bmatrix}
\end{bmatrix}
D^{\beta}
\begin{Bmatrix}\mathbf{q}_1\\ \mathbf{q}_2\\ \mathbf{q}_3\\ \mathbf{q}_4\\ \vdots\\ \mathbf{q}_{n\cdot N-1}\\ \mathbf{q}_{n\cdot N}\end{Bmatrix} +
$$

$$
\begin{bmatrix}
\begin{bmatrix}\mathbf{M}_{(1)_1}\end{bmatrix} & & & & & \\
& \begin{bmatrix}\mathbf{M}_{(2)_2}\end{bmatrix} & & & & \\
& & \begin{bmatrix}\mathbf{M}_{(3)_3}\end{bmatrix} & & & \\
& & & \ddots & & \\
& & & & \begin{bmatrix}\mathbf{M}_{(N-1)_{N-1}}\end{bmatrix} & \\
& & & & & \begin{bmatrix}\mathbf{M}_{(N)_N}\end{bmatrix}
\end{bmatrix}
\frac{d^2}{dt^2}
\begin{Bmatrix}\mathbf{q}_1\\ \mathbf{q}_2\\ \mathbf{q}_3\\ \mathbf{q}_4\\ \vdots\\ \mathbf{q}_{n\cdot N-1}\\ \mathbf{q}_{n\cdot N}\end{Bmatrix} =
\begin{Bmatrix}\mathbf{Q}_1\\ \mathbf{Q}_2\\ \mathbf{Q}_3\\ \mathbf{Q}_4\\ \vdots\\ \mathbf{Q}_{n\cdot N-1}\\ \mathbf{Q}_{n\cdot N}\end{Bmatrix}
\tag{46}
$$